

Nonequilibrium calcium dynamics optimizes the energetic efficiency of mitochondrial metabolism

Valérie Voorsluijs^{1,2}, Francesco Avanzini^{2,3}, Gianmaria Falasco^{2,4}, Massimiliano Esposito², Alexander Skupin^{1,5,6}

***For correspondence:**

valerie.voorsluijs@uni.lu (VV);
francesco.avanzini@unipd.it (FA);
gianmaria.falasco@unipd.it (GF);
massimiliano.esposito@uni.lu (ME);
alexander.skupin@uni.lu (AS)

¹Luxembourg Centre for Systems Biomedicine, University of Luxembourg, 6 avenue du Swing, L-4367 Belvaux, Luxembourg; ²Complex Systems and Statistical Mechanics, Department of Physics and Materials Science, University of Luxembourg, 162A avenue de la Faiënerie, L-1511 Luxembourg, Luxembourg; ³Department of Chemical Sciences, University of Padova, 1 Via F. Marzolo, I-35131 Padova, Italy; ⁴Department of Physics and Astronomy, University of Padova, 8 Via F. Marzolo, I-35131 Padova, Italy; ⁵Department of Physics and Materials Science, University of Luxembourg, 162 A avenue de la Faiënerie, L-1511 Luxembourg, Luxembourg; ⁶Department of Neuroscience, University of California San Diego, 9500 Gilman Drive, 92093 San Diego, CA, USA

Abstract Living organisms continuously harness energy for their survival while part of that energy is dissipated, and determining the efficiency of specific cellular processes remains a largely open problem. Here, we analyze the efficiency of ATP production through the Krebs cycle and oxidative phosphorylation, which generate most of the chemical energy in eukaryotes. The regulation of this pathway by calcium signaling can affect its energetic output, but the concrete energetic impact of this crosstalk remains elusive. Calcium enhances ATP production by activating key enzymes of the Krebs cycle while calcium homeostasis is ATP-dependent. We propose a detailed kinetic model describing the calcium-mitochondria crosstalk and analyze it using nonequilibrium thermodynamics: after identifying the effective reactions driving mitochondrial metabolism out of equilibrium, we quantify the thermodynamic efficiency of mitochondrial metabolism for different physiological conditions. Calcium oscillations boost the efficiency close to substrate-limited conditions, suggesting a compensatory role of calcium signaling in mitochondrial bioenergetics.

Introduction

Life relies on permanent conversions between different forms of energy, a phenomenon referred to as energy transduction. A wide range of cellular processes are fueled by the chemical energy stored in adenosine triphosphate (ATP), but the compartmentalization of eukaryotic cells also enables the storage of potential energy across the membranes of organelles (*Nicholls and Ferguson, 1992*). Energy transduction is mediated by enzymes and pumps driven in a nonequilibrium thermodynamic manner by the hydrolysis of ATP, chemical gradients or membrane potentials.

In optimal scenarios where transduction is fully efficient, the input energy is completely transformed into usable work. However, biological processes are typically accompanied by entropy production, *i.e.*, dissipation of energy in the form of heat and/or chemical waste that is unusable for transduction (*Calisto et al., 2021*). For example, the action of many transmembrane ionic pumps

transporting ions against their concentration gradient is often based on catalysing the hydrolysis of ATP. The chemical energy released by hydrolysis is partly used to drive ionic transport while another part is dissipated. In the extreme case of pump uncoupling, also known as “slippage”, all the energy of ATP hydrolysis is dissipated without any ion transport (*Berman, 2001*).

Different nonequilibrium kinetic models have been developed to account for energy loss in pumps (*Gräber and Milazzo, 1997; Rubi et al., 2007; Hill, 2012; Wikström and Springett, 2020*) but have only provided limited insights into energetic costs at the pathway level. New approaches based on metabolic network reconstruction and nonequilibrium thermodynamics are gradually emerging to rationalize the energetic costs of cellular processes (*Yang et al., 2021*) including gene regulation (*Estrada et al., 2016*), repair mechanisms (*Sartori and Pigolotti, 2015; Goloubinoff et al., 2018*), enzymatic catalysis (*Flamholz et al., 2013*), information processing (*Parrondo et al., 2015*) or signaling (*Cao et al., 2015; Rodenfels et al., 2019*). A framework to study energy transduction in complex open chemical reaction networks (CRN) has recently been proposed and used to study the efficiency of pathways of the central energy metabolism in the absence of regulations (*Wachtel et al., 2022*). Evaluating the efficiency of tightly coupled transduction processes, *i.e.* processes whose input and output currents are equal, is straightforward as it does not depend on the net reaction flux. However, when regulations come into play, this tight coupling can be lost and kinetic models become indispensable to evaluate the flux of the different processes contributing to the efficiency.

Here, we resort to a such a kinetically-detailed nonequilibrium thermodynamic approach to show and quantify how active signaling can have a beneficial energetic impact on metabolism. In particular, we analyze the efficiency of the mitochondrial production of ATP *via* the tricarboxylic acid (TCA) cycle and oxidative phosphorylation (OXPHOS), and take into account its regulation by calcium (Ca^{2+}). In mitochondria, Ca^{2+} activates two key enzymes of the TCA cycle (isocitrate dehydrogenase and α -ketoglutarate dehydrogenase) (*McCormack, 1985; Hajnóczky et al., 1995; Griffiths and Rutter, 2009; Denton, 2009*) and thereby increases the flux of high energy electrons, in the form of NADH, feeding the electron transport chain. The successive redox reactions in the mitochondrial membrane contribute to the establishment of the proton motive force driving the mitochondrial synthesis of ATP by F1F0-ATPase. Depending on the concentration of cytosolic ATP, Ca^{2+} can, however, be sequestered into cell compartments other than mitochondria, such as the endoplasmic reticulum (ER) *via* the sarcoendoplasmic reticulum Ca^{2+} ATPase (SERCA), or extruded to the extracellular space (*Berridge et al., 1998*). These mechanisms ensure that Ca^{2+} does not accumulate in the cytosol, as a persistent high cytosolic Ca^{2+} concentration is toxic for the cell. The central coupling enabling the Ca^{2+} -mitochondria crosstalk is thus given by the Ca^{2+} fluxes between the cytosol and the ER or mitochondria (*Figure 1*). The Ca^{2+} release from the ER, by leakage or *via* channels (IP₃Rs) upon stimulation by inositol 1,4,5-trisphosphate (IP₃), and Ca^{2+} exchanges with mitochondria are ATP-independent, as opposed to Ca^{2+} transport into the ER that relies on ATP-consuming SERCA pumps.

Since intracellular Ca^{2+} dynamics is strongly nonlinear (which can lead to oscillations in Ca^{2+} concentration) and depends itself on ATP availability, evaluating the net effect of signaling on the energetic efficiency of mitochondrial metabolism is not straightforward. Our analysis quantifies the energetic efficiency of this essential cellular process beyond steady-state conditions, such as in an oscillatory regime. Overall, the proposed framework is laying the foundations for a more comprehensive characterization of energetic costs in biology.

Results

Modeling and theoretical frameworks

We developed a curated model for the essential Ca^{2+} -metabolism system integrating different modules (*Magnus and Keizer, 1997, 1998a,b; Dudycha, 2000; Cortassa et al., 2003; Bertram et al., 2006; Wei et al., 2011; Komin et al., 2015; Berndt et al., 2015; Wacquier et al., 2016*). Its comprehensive parameterization on experimental data represent a major step towards the detailed analysis of

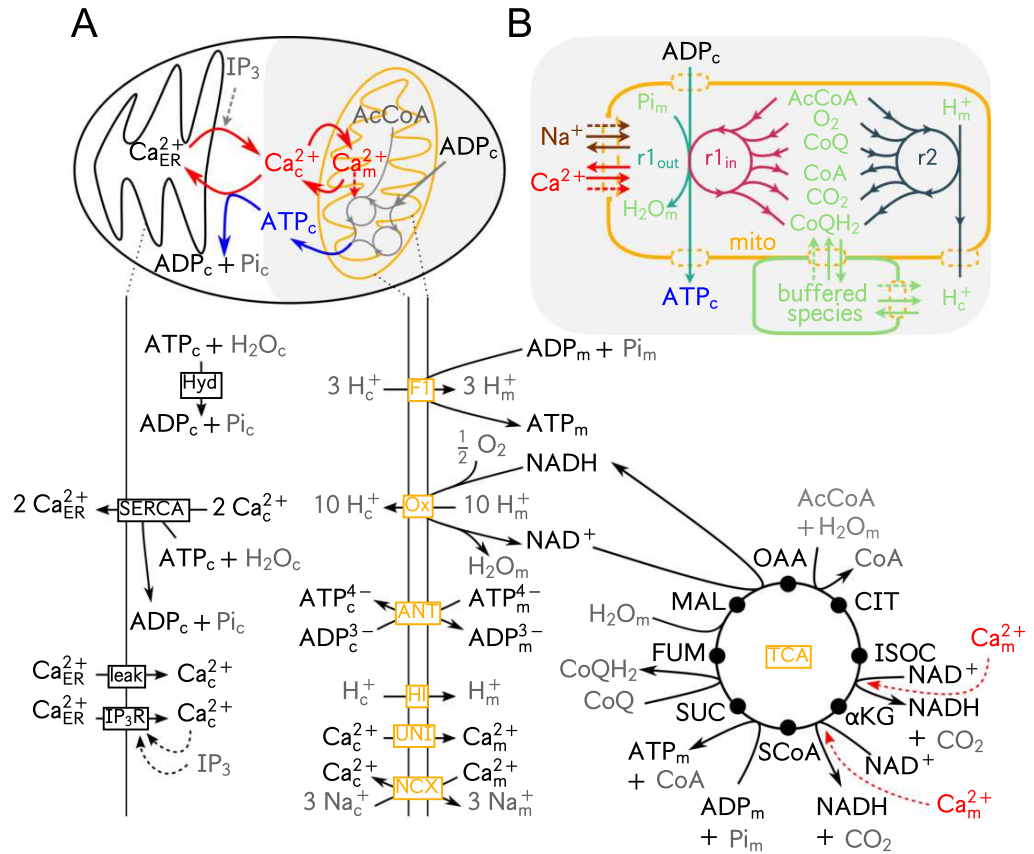


Figure 1. Representation of the model components, conceptualization of mitochondria as a chemical engine and corresponding abbreviations. Balanced chemical equations, detailed expressions of the reaction rates, thermodynamic forces and reference parameter values are given in [Table 1](#), [Table 2](#), [Table 3](#) and [Table 4](#) in Methods, respectively. (A) The upper part depicts the Ca^{2+} (red) and ATP (blue) fluxes responsible for the crosstalk between Ca^{2+} dynamics and mitochondrial metabolism. The bottom part is a detailed description of the model components. The kinetic rates for TCA cycle fluxes and processes involving exchanges across the mitochondrial membrane are respectively originating from Dudycha ([Dudycha, 2000](#)) and Magnus-Keizer models ([Magnus and Keizer, 1997, 1998a,b](#)), except for the transformation of MAL into OAA, which is described more realistically by a reversible flux ([Berndt et al., 2015](#)). Here, OXPHOS corresponds to the net redox reaction resulting from the electron transport chain (Ox) and the synthesis of ATP by the F1F0-ATPase (F1). A last module, consisting of Ca^{2+} exchanges across the ER membrane and cytosolic ATP hydrolysis are taken from the models from Komin *et al.* ([Komin et al., 2015](#)) and from Wacquier *et al.* ([Wacquier et al., 2016](#)). Controlled species (*i.e.*, species whose concentration is assumed to be constant) are shown in gray, dynamical species in black and dashed arrows represent regulations. Processes are annotated in yellow and black boxes for mitochondrial and cytosolic/ER processes, respectively. (B) Mitochondrial metabolism is conceptualized as an open chemical engine that transforms ADP_c into ATP_c through a set of 2 emergent cycles split in 3 effective reactions ($r_{1_{\text{out}}}$, $r_{1_{\text{in}}}$ and r_2). Some of the controlled species involved in the internal reactions are buffered at a constant concentrations (green), while Na^+ (brown) and Ca^{2+} (red) regulate reaction rates by activating specific enzymes or acting on the mitochondrial membrane potential. Abbreviations: AcCoA – acetyl coenzyme A, αKG – alpha-ketoglutarate, ATP – Adenosine triphosphate, ADP – Adenosine diphosphate, CIT – citrate, CoA – coenzyme A, CoQ/COQH₂ – coenzyme Q10, FUM – fumarate, IP₃ – inositol 1,4,5-trisphosphate, ISOC – isocitrate, MAL – malate, NAD⁺/NADH – nicotinamide adenine dinucleotide, OAA – oxaloacetate, Pi – inorganic phosphate, SUC – succinate, SCoA – succinyl coenzyme A.

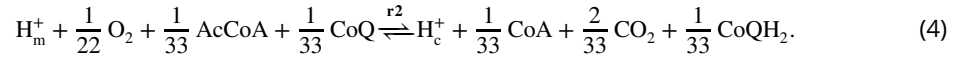
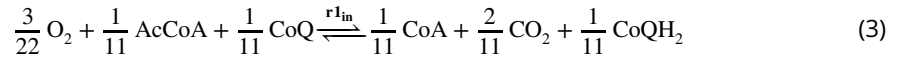
the mitochondrial regulation by Ca^{2+} . The underlying kinetic models originally aimed at capturing the essential mechanisms of the the Ca^{2+} -metabolism interplay and at rationalizing experimental data about the response of Ca^{2+} signals to changes in mitochondrial activity (and *vice versa*). After refining these models to combine them in a coherent way, we analyzed the coupled pathways by a nonequilibrium thermodynamic description of CRN (*Rao and Esposito, 2016, 2018; Wachtel et al., 2018; Avanzini et al., 2020, 2021; Avanzini and Esposito, 2022; Avanzini et al., 2023; Wachtel et al., 2022*).

To compute their metabolic efficiency, we analyzed mitochondria as out-of-equilibrium chemical engines (*Figure 1B*) satisfying the second law of thermodynamics (*Rao and Esposito, 2018; Avanzini et al., 2021*):

$$T\sigma = -d_t \mathcal{G} + \dot{w}_{\text{nc}} + \dot{w}_{\text{driv}}. \quad (1)$$

Mitochondrial metabolism constitutes an open CRN that continuously harnesses the free energy stored in buffered species (e.g., AcCoA, CoQ, O_2 , H^+) to synthesize ATP_c from ADP_c while being influenced by Na^+ homeostasis and cytosolic processes such as Ca^{2+} signaling and ATP_c consumption. From a thermodynamic perspective, the synthesis of ATP_c and the regulations correspond to free energy exchanges between the mitochondrial engine and its surroundings. They appear in the second law (*Equation 1*) as the nonconservative work rate, \dot{w}_{nc} , and the driving work rate, \dot{w}_{driv} , respectively. \dot{w}_{nc} is the energy current maintaining the CRN out of equilibrium while \dot{w}_{driv} is the energy current resulting from the modification of the underlying equilibrium state by the out-of-equilibrium dynamics (*Figure 3B*). The difference between their sum and the variation in time of the internal Gibbs free energy of mitochondria, \mathcal{G} , equals the free energy dissipated by the mitochondrial reactions, *i.e.* the entropy production rate (EPR) σ times the absolute temperature T .

The expressions of the thermodynamic quantities in *Equation 1* are derived for mitochondrial metabolism using a topological analysis (developed in *Avanzini et al. (2020, 2021, 2023)*) of the corresponding CRN, which allowed us to identify conservation laws and emergent cycles. The conservation laws define parts of molecules that remain intact in all mitochondrial reactions and are instrumental to determine the Gibbs free energy \mathcal{G} . The emergent cycles define the 3 effective reactions



and split the nonconservative work rate into the sum of 3 contributions: $\dot{w}_{\text{nc}} = \dot{w}_{r_{1,\text{out}}} + \dot{w}_{r_{1,\text{in}}} + \dot{w}_{r_2}$, where $\dot{w}_{r_{1,\text{out}}}$ quantifies the mitochondrial free energy output corresponding to the synthesis of ATP in the cytosol (*Equation 2*), while $\dot{w}_{r_{1,\text{in}}}$ and \dot{w}_{r_2} quantify the mitochondrial free energy power source due the interconversion of the buffered species *via* reactions in *Equation 3* and *Equation 4*, respectively.

The average thermodynamic efficiency $\bar{\eta}$ of mitochondria can then be calculated as

$$\bar{\eta} = -\frac{\overline{\dot{w}_{\text{nc}}^{\text{output}}}}{\overline{\dot{w}_{\text{nc}}^{\text{input}}} + \overline{\dot{w}_{\text{driv}}}} \quad (5)$$

where $\overline{\dot{w}_{\text{nc}}^{\text{input}}} = \overline{\dot{w}_{r_{1,\text{in}}} + \dot{w}_{r_2}}$ and $\overline{\dot{w}_{\text{nc}}^{\text{output}}} = \overline{\dot{w}_{r_{1,\text{out}}}}$, and the overline denotes either steady-state quantities or averages over one period of Ca^{2+} oscillations (notice that $d_t \mathcal{G} = 0$).

The EPR nonconservative and driving work contributions vanish at equilibrium according to the second law of thermodynamics but take finite values in nonequilibrium regimes (*Figure 3B*). The nonequilibrium kinetics of the system was assessed for different stimulation conditions and mitochondrial substrate concentrations (*i.e.* for different $[\text{IP}_3]$ and $[\text{AcCoA}]$ in the simulations), which allowed for the calculation of the corresponding nonconservative and driving work contributions and, ultimately, of the efficiency of mitochondrial metabolism.

Ca²⁺-metabolism crosstalk affects the oscillation period and the production of ATP

To validate the kinetic model, we compared our simulation results to experimental and simulation data from the literature. Slow spiking is found around the bifurcation point corresponding to the transition from steady-state to oscillations, which marks the onset of the signaling machinery. A decrease in the oscillation period is observed as $[IP_3]$ is increased (Figure 2A-C) or as $[AcCoA]$ is decreased (Figure 2C). These trends are in agreement with stimulation experiments performed in various cell types (Woods et al., 1986; Falcke, 2004; Dupont et al., 2007; Thurley et al., 2014; Moein, 2017) and with behaviors reported for limited availability of mitochondrial substrate (Jouaville et al., 1995; Wacquier et al., 2016; Moein, 2017). In the oscillatory regime, $[ATP]_c$ displays a maximum in dependence on $[IP_3]$ and $[AcCoA]$ (Figure 2D-E and Figure 3—figure Supplement 2), a feature that is also predicted by the model of Wacquier et al. (Wacquier et al., 2016). In our simulations, a cusp in the average of $[ATP]_c$ is additionally observed at the critical point (Figure 2D-E).

Most of these observations can be rationalized based on the dependence of SERCA pumps on ATP_c , which enables the switch between ER and mitochondrial Ca^{2+} sequestration and is a key signature of the Ca^{2+} -metabolism crosstalk. As $[IP_3]$ increases, more Ca^{2+} is released into the cytosol through IP_3 Rs. The steady-state $[ATP]_c$ thus decreases due to a more demanding maintenance of the basal $[Ca^{2+}]_c$ via SERCA pumps. At the critical $[IP_3]$ corresponding to the onset of oscillations, mitochondrial sequestration of Ca^{2+} becomes significant, which not only relieves SERCA pumps but also enables the activation of Ca^{2+} -sensitive dehydrogenases of the TCA cycle (Figure 2—figure Supplement 1). These combined effects result in an increase of the average $[ATP]_c$. Increasing $[IP_3]$ further leads to saturation in mitochondrial buffering of Ca^{2+} (Figure 2—figure Supplement 1). More intense Ca^{2+} sequestration via SERCA pumps is then required and the associated ATP_c consumption is no longer counterbalanced by the Ca^{2+} -enhanced mitochondrial activity, which results in a slow decrease in average $[ATP]_c$. Meanwhile, increasing stimulation by IP_3 favors more frequent opening of the IP_3 Rs, which results in a decrease of the oscillation period. In most mathematical models for Ca^{2+} signaling and in agreement with experimental observations, the oscillation period saturates at high $[IP_3]$ (Eisner and Valdeolmillos, 1986) and, beyond a critical $[IP_3]$, oscillations disappear. The cell then exhibits a high- $[Ca^{2+}]_c$ steady-state (Falcke, 2004), as reproduced by our simulations (Figure 2—figure Supplement 1). Further stimulation by IP_3 does not affect the steady-state concentrations reached after termination of the oscillations (see Figure 3C bottom for $[ATP]_c$ and Figure 2—figure Supplement 1 for $[Ca^{2+}]_c$ and $[Ca^{2+}]_m$), suggesting that IP_3 Rs have reached their maximal release rate and contribute to saturation effect.

The impact of $AcCoA$ level on $[ATP]_c$ and oscillation period is more visible in starving conditions, i.e. $[AcCoA] \leq 1 \mu M$, and for low stimulation by IP_3 , i.e. $[IP_3] \leq 0.24 \mu M$. ATP production decreases as $[AcCoA]$ is decreased except at the onset of oscillations, where a cusp in $[ATP]_c$ occurs (Figure 2E and Figure 2—figure Supplement 1B). At this critical point, $[ATP]_c$ has become limiting for Ca^{2+} uptake by SERCAs and mitochondrial exchanges take over. This switch allows for activation of TCA cycle enzymes by Ca^{2+} and locally rescues ATP production. Mitochondrial exchanges intensify as $[AcCoA]$ is further decreased. The larger Ca^{2+} efflux from mitochondria exerts a positive feedback on IP_3 Rs which open more frequently, hence the decrease in oscillation period.

The efficiency of mitochondrial metabolism displays a maximum in the regime of Ca^{2+} spiking

The nonlinear ATP production (Figure 2D-E) observed for different $[IP_3]$ and $[AcCoA]$ suggests variations in the output work of mitochondria and, possibly, in the thermodynamic efficiency of their metabolism. As confirmed computationally, the output nonconservative work ($\bar{w}_{r,out}$) displays a minimum (corresponding to maximal export of energy from mitochondria) that coincides with the maximal $[ATP]_c$ in the kinetic simulations (Figure 3A and Figure 3—figure Supplement 2A top, vs Figure 3C and Figure 3—figure Supplement 2B bottom). In the extreme case where oscillations disappear for large stimulation by IP_3 , the efficiency drops and reaches a plateau (Figure 3E top). On the other hand, both the non-conservative input work contributions ($\bar{w}_{r,in}$ and $\bar{w}_{r,2}$) increase

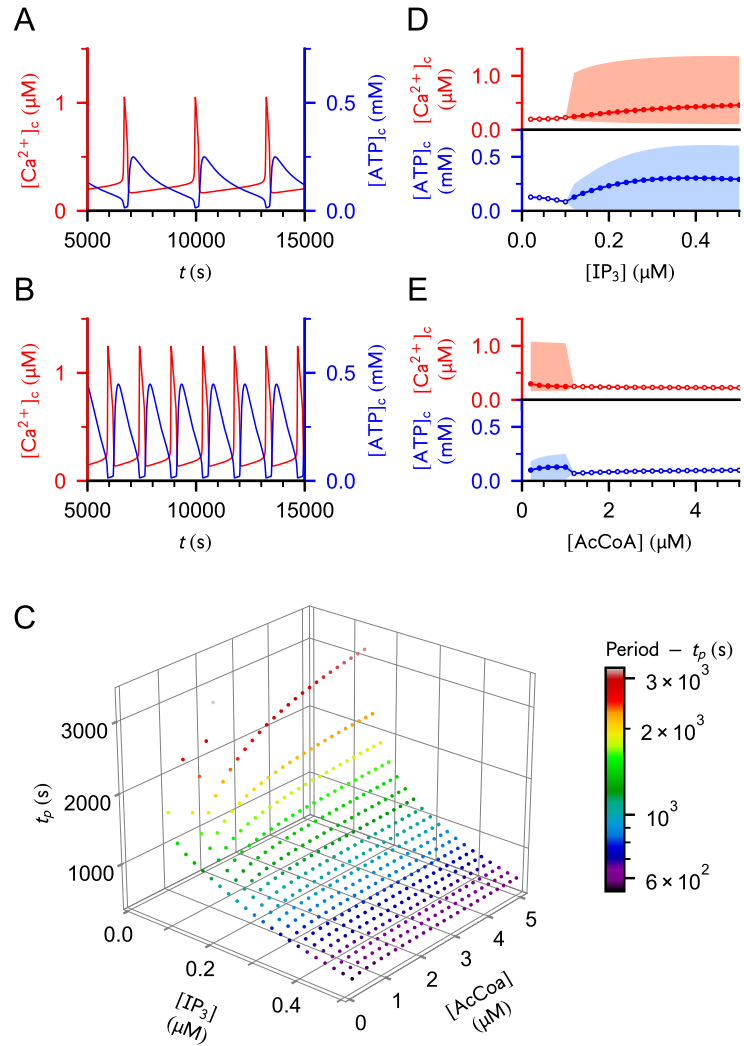


Figure 2. Kinetic behavior of the system. (A-B) Ca^{2+} and ATP_c concentrations over time for $[AcCoA] = 1 \mu\text{M}$ and (A) $[IP_3] = 0.12 \mu\text{M}$ or (B) $[IP_3] = 0.20 \mu\text{M}$. (C) Effect of $[IP_3]$ and $[AcCoA]$ on the oscillation period. (D-E) Average concentration of Ca^{2+} and ATP_c as a function of (D) $[IP_3]$ for $[AcCoA] = 1 \mu\text{M}$ or as a function of (E) $[AcCoA]$ for $[IP_3] = 0.12 \mu\text{M}$. Empty and filled dots represent steady-state and oscillatory regimes, respectively, and the boundaries of the shaded areas correspond to the minimum and maximum concentrations. Parameter values are given in [Table 4](#). [Figure 3—figure Supplement 1B](#) illustrates the behavior of $[ATP]_c$ for an extended range of $[AcCoA]$ and $[IP_3]$.

Figure 2—figure supplement 1. Average SERCA, UNI and Ca^{2+} -dependent TCA fluxes and average cytosolic and mitochondrial Ca^{2+} concentrations vs. $[IP_3]$ as complementary figures to the bifurcation diagrams shown in [Figure 2D](#) and [Figure 3C](#) bottom and portrait phases in [Figure 4C](#). Note that \bar{J}_{IDH} and \bar{J}_{KGDH} are indistinguishable. Empty and filled dots correspond to steady-state or period-averaged quantities, respectively. Parameter values are the same as in [Figure 2D](#).

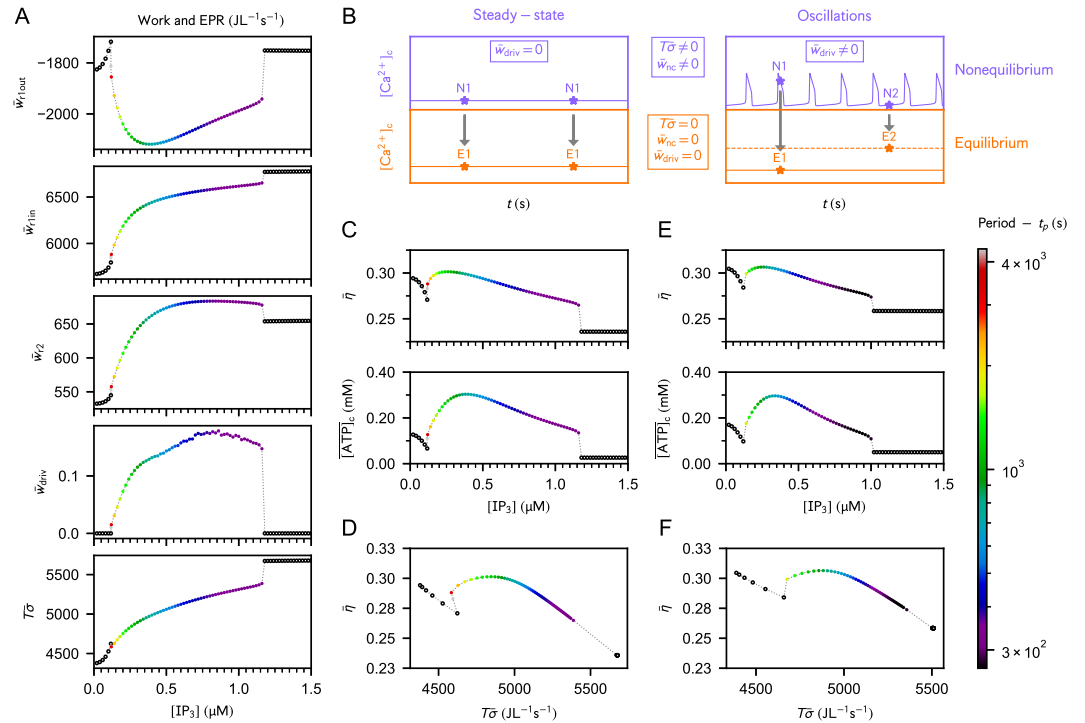


Figure 3. Stimulating the Ca²⁺ signaling machinery impacts the dissipation and efficiency of mitochondrial metabolism *via* the Ca²⁺-metabolism crosstalk. (A) Nonconservative work contributions, driving work and dissipation for different [IP₃]. The driving work represents less than 0.01% of the EPR. At high stimulation, oscillations disappear in the favor of a nonequilibrium steady-state regime. (B) Expected work contributions in equilibrium and nonequilibrium conditions. Stars denote the state of the system at different time points in nonequilibrium conditions (violet) and the corresponding underlying equilibrium state (orange). As illustrated, the non-zero driving work contribution in the oscillatory regime can modify the underlying equilibrium state of the system. (C) Efficiency and ATP_c concentration as a function of [IP₃]. (D) Efficiency as a function of the total dissipation for a range of [IP₃] extended up to 5 μM. (E-F) Plots corresponding to (C-D) for $V_{max}^{SERCA} = 0.08 \mu\text{M s}^{-1}$. Empty and filled dots correspond to steady-state or period-averaged quantities, respectively. Unless specified otherwise, parameter values are the same as in **Figure 2D**. An analogous thermodynamic behavior is observed upon stimulation by AcCoA (**Figure 3—figure Supplement 2**).

Figure 3—figure supplement 1. Efficiency of mitochondrial metabolism (η), average cytosolic ATP concentration ($\overline{[\text{ATP}]_c}$ (mM)) and period of Ca²⁺ oscillations (t_p) as functions of [AcCoA] and [IP₃]. (A-B) Summary 3D plots. IP₃ plays a dominant role in the transition between steady-state and oscillations, which usually takes place for concentrations of IP₃ between 0.1 and 0.2 μM. The onset of oscillations can be triggered for smaller [IP₃] in the presence of a very low level of AcCoA (e.g. [AcCoA] = 0.2 μM), which supports the role of Ca²⁺ oscillations as a rescuing mechanism aiming to improve the efficiency of energy production in stressing situations such as limited access to carbon substrate. For more clarity, representative behaviors of the efficiency (top panels), $\overline{[\text{ATP}]_c}$ (mM) (middle panels) and period (low panels) were plot for (grey lines - C) [AcCoA] = 1 μM and (brown lines - D) [IP₃] = 0.12 μM, as complementary figures to the bifurcation diagrams shown in Fig. 2E and 2F, respectively. Note that maxima in efficiency and in $\overline{[\text{ATP}]_c}$ (mM) can also be observed when [AcCoA] is varied. Increments in concentrations are of 0.2 μM (A-B) or 0.1 μM (D) for AcCoA and of 0.2 μM (A - C) for IP₃.

Figure 3—figure supplement 2. Stimulation of mitochondrial metabolism by AcCoA impacts Ca²⁺ dynamics *via* the Ca²⁺-metabolism crosstalk. (A) Nonconservative work contributions, driving work and dissipation for different [AcCoA]. The driving work represents less than 0.0004% of the EPR. At high stimulation, oscillations disappear in the favor of a nonequilibrium steady-state regime. (B) Efficiency and ATP_c concentration as a function of [IP₃]. (C) Efficiency as a function of the total dissipation for the same range of [AcCoA] as in (A) and (B). (D-E) Plots corresponding to (B-C) for $V_{max}^{SERCA} = 0.08 \mu\text{M s}^{-1}$. Empty and filled dots correspond to steady-state or period-averaged quantities, respectively. Unless specified otherwise, parameter values are the same as in **Figure 2D**.

with $[IP_3]$ and $[AcCoA]$, while the driving work (\bar{w}_{driv}) is always negligible compared to the total dissipation (**Figure 3A** and **Figure 3—figure Supplement 2A**).

Importantly, the maximum in $[ATP]_c$ translates into a maximum in the efficiency of mitochondrial metabolism (**Figure 3C** and **Figure 3—figure Supplement 2B**). Such maxima are not systematically observed when $[AcCoA]$ is varied at fixed $[IP_3]$ (**Figure 2—figure Supplement 1A-B**). However, the increase in efficiency at the onset of the oscillatory regime is a robust feature that points to the stabilizing effect of Ca^{2+} spikes on mitochondrial energetics.

The relation between mitochondrial efficiency and dissipation is different in fast Ca^{2+} spiking regimes triggered by starvation or overstimulation by IP_3

Like in other biological processes such as the migration of molecular motors along microtubules, kinetic proofreading or the regulation of circadian clocks (*Baiesi and Maes, 2018*), the system's efficiency is maximal at intermediate levels of dissipation, corresponding to a limited range of $[IP_3]$ and $[AcCoA]$ (**Figure 3E** and **Figure 3—figure Supplement 2D**).

Overstimulation of the signaling machinery by IP_3 is counterproductive since it only increases dissipation (**Figure 3A** bottom). By exploring the behavior of efficiency and EPR at large $[IP_3]$, we observed a saturation effect (**Figure 3A, C** and **D**) leading to limiting values for the efficiency (≈ 0.236) and total dissipation ($\approx 5680 \text{ JL}^{-1}\text{s}^{-1}$). The dependency of efficiency on the total dissipation is highly nonlinear (**Figure 3D**). Around the onset of oscillations (and for a limited range of dissipation rates), a given dissipation rate can be associated to different efficiencies, in which case the highest efficiency is always reached for the highest Ca^{2+} spiking frequency, while the lowest efficiency corresponds to the steady-state regime. Reversely, different dissipative regimes can yield the same efficiency. In that case, steady-state regimes display the lowest EPR while the fast-spiking regimes are the more dissipative regimes. We hypothesize that in such instances, the selection of the dissipative regime could be guided by constraints imposed by the global energy budget of the cell.

As $[AcCoA]$ is increased, slow-spiking regimes are more dissipative than the fast-spiking ones (**Figure 3—figure Supplement 2A**, bottom panel) and the efficiency increases almost linearly with dissipation in the oscillatory regime (**Figure 3—figure Supplement 2C**), which contrasts with the overstimulation by IP_3 . A reason for this difference might be that upon overstimulation by IP_3 , ATP_c hydrolysis overbalances the enhanced production of ATP by mitochondrial metabolism, which is not the case at low $[AcCoA]$.

To summarize, fast spiking is less efficient than the slow spiking observed around the bifurcation point, and is also more dissipative when oscillations frequency intensifies due to perturbations in $[IP_3]$.

Robustness of the efficiency-rescuing effect of Ca^{2+} oscillations

Our proposed mechanism for the maximum in efficiency relies on the dependence of the SERCA flux (J_{SERCA}) on the hydrolysis of ATP_c and on the resulting modulation of Ca^{2+} sequestration mechanisms. If Ca^{2+} homeostasis was ATP-independent, Ca^{2+} would always exert a positive feedback on the TCA cycle flux and the efficiency of metabolism would increase monotonically with the Ca^{2+} release from IP_3 Rs. We validated this hypothesis by performing simulations with a modified SERCA flux that is uncoupled from ATP_c hydrolysis. The degradation of ATP_c then relies exclusively on other ATP-consuming processes mimicking cellular activity (Hyd reaction in **Figure 1A**). As expected, the Ca^{2+} -enhanced ATP production by mitochondria is not restrained upon more intense stimulation by IP_3 (**Figure 4A**). This uncoupling also disables the feedback of ATP production by mitochondria on Ca^{2+} oscillations: instead of decreasing, the spike period is barely changed as $[AcCoA]$ decreases (**Figure 4B**).

In the uncoupled case, J_{SERCA} is not limited by the depletion of ATP_c and both removal mechanisms proceed synchronously, although Ca^{2+} uptake to the ER is predominant (**Figure 4C**, green dotted curve). While the mitochondrial Ca^{2+} influx J_{UNI} slightly increases with J_{SERCA} , the Ca^{2+} -dependent currents of the TCA cycle, J_{IDH} and J_{KGDH} (**Figure 4C**, purple dotted curves), are barely

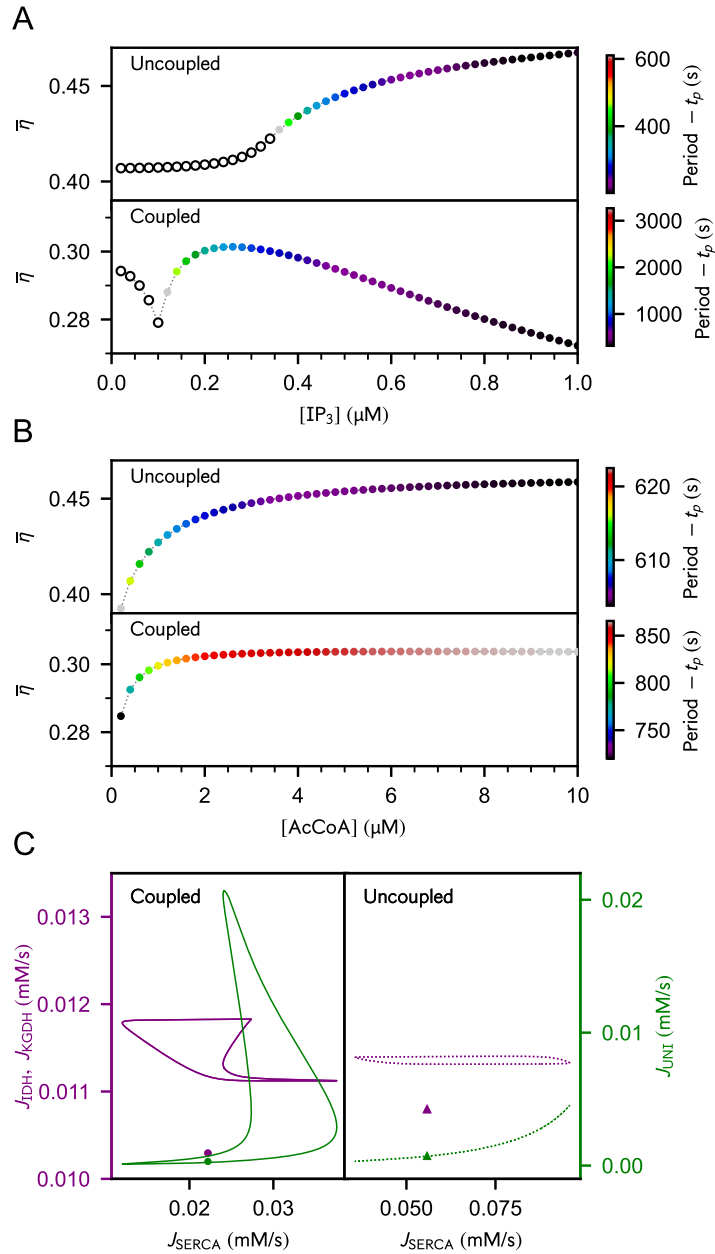


Figure 4. Efficiency of mitochondrial metabolism regulated by Ca^{2+} signaling, Ca^{2+} sequestration fluxes and Ca^{2+} -dependent TCA cycle reaction fluxes, without and with the coupling of SERCA pumps to ATP_c hydrolysis. (A) Stimulating Ca^{2+} release by IP_3 Rs (that is, increasing $[\text{IP}_3]$) monotonically increases the efficiency in the uncoupled case, which strongly contrasts with the nonmonotonic dependency on $[\text{IP}_3]$ in the coupled case. While varying over different ranges, the period evolves according to the same trends in both cases. (B) Both systems display similar responses in their efficiency upon variations in $[\text{AcCoA}]$, but the oscillation period of the uncoupled system does not decrease – and is even slightly increasing – in stressing conditions corresponding to substrate depletion. As this observation is in contradiction with experimental evidence, the larger efficiencies reached in the uncoupled case are non physiological. Empty and filled dots correspond respectively to steady-state and oscillatory regimes – note the use of linear colorbar schemes for the period. (C) Phase portraits of Ca^{2+} -dependent TCA cycle currents (purple) and mitochondrial Ca^{2+} uptake (green), namely $J_{\text{IDH}}, J_{\text{KGDH}}$ and J_{UNT} , vs. ER Ca^{2+} uptake, namely J_{SERCA} . Note that J_{IDH} and J_{KGDH} are indistinguishable. Symbols denote steady-state values. Triangles ($[\text{IP}_3] = 0.34 \mu\text{M}$) and dotted curves ($[\text{IP}_3] = 0.42 \mu\text{M}$) correspond to the uncoupled case, while circles ($[\text{IP}_3] = 0.10 \mu\text{M}$) and solid curves ($[\text{IP}_3] = 0.24 \mu\text{M}$) represent the coupled case. (A and C) $[\text{AcCoA}] = 1 \mu\text{M}$, (B) $[\text{IP}_3] = 0.36 \mu\text{M}$ and the other parameter values are the same as in *Figure 2–Figure 3*.

affected. Upon regulation by ATP_c , J_{SERCA} varies over a more restricted range, is on average smaller and proceeds with a slight phase shift with respect to J_{UNI} , which allows for a larger Ca^{2+} influx in mitochondria and a more intense activation of the TCA cycle enzymes (**Figure 4C** solid curves). This mechanism supports the “efficiency-rescuing” role of mitochondrial buffering that is visible near the onset of oscillations in the coupled case (**Figure 3C** and **Figure 4A** bottom), while no such cusp-like transition is observed in the uncoupled case (**Figure 4A** top).

We also explored the robustness of our results against perturbations in the uptake rate of SERCA pumps of the original model. We mimicked the inhibition of SERCA pumps by decreasing the limiting rate $V_{\text{max}}^{\text{SERCA}}$. The efficiency-dissipation relation displays the same features as in the non-inhibited case (**Figure 3F** and **Figure 3—figure Supplement 2E** vs **Figure 3D** and **Figure 3—figure Supplement 2C**, respectively).

Together, these results confirm that the crosstalk between Ca^{2+} signaling and mitochondrial energy metabolism is a major mechanism underlying the maximum in efficiency arising in the spiking regime, even when the amplitude of this coupling is reduced due to the inhibition of SERCA pumps.

Discussion

Here, we examined the impact of Ca^{2+} signaling on the efficiency of mitochondrial metabolism by using tools from the nonequilibrium thermodynamics of CRNs on a detailed and experimentally validated kinetic model of the Ca^{2+} -metabolism crosstalk. Our results highlight that, despite a usually higher dissipation rate compared to steady-state regimes, Ca^{2+} oscillations can enhance the efficiency of mitochondrial metabolism. In particular, stimulation by IP_3 reduces the steady-state efficiency of metabolism but at the onset of oscillations the efficiency raises with a cusp-like transition and reaches a maximum of about 30% before decreasing again at higher stimulation. This value corresponds to the efficiency of the TCA cycle estimated in the absence of regulation with a nonequilibrium thermodynamic approach (**Wachtel et al., 2022**). Moreover, slow-spiking is less dissipative than fast-spiking. Thus, we hypothesize that, for a given cell state, there exists an optimal stimulation level leading to slow-spiking/low-dissipation oscillations which maximize the efficiency of metabolism during signaling. For higher stimulation, the Ca^{2+} signaling machinery then generates more dissipative regimes of gradually decreasing efficiency.

In the broader context of physical bioenergetics, energetic costs are usually assessed by evaluating the Gibbs free energy of reaction ($\Delta_r G$) dissipated or the equivalent number of ATP molecules produced/consumed along the processes of interest (**Cao et al., 2015; Rodenfels et al., 2019; Yang et al., 2021**). However, such purely thermodynamic approaches do not account for reaction kinetics and thus cannot quantify the rates of free energy transduction and dissipation. Significant efforts have been made in the direction of adding thermodynamic constraints in flux balance analysis of metabolic networks (**Beard et al., 2002; Niebel et al., 2019**). A few attempts have also been made to account for more complex kinetic effects such as enzyme saturation, leading to insights into the trade-offs between energy production and enzyme costs in glycolysis (**Noor et al., 2013a; Flamholz et al., 2013; Stettner and Segrè, 2013**). Nevertheless, all these approaches rely on optimized nonequilibrium steady-states, which may not correspond to physiological conditions and cannot capture the energetic impact of time-dependent behaviors, such as the energy-rescuing effect of Ca^{2+} oscillations quantified here. Our approach overcomes these limitations, based on the rigorous thermodynamic analysis of a curated dynamical model. Due to the modular structure of the model, our approach can be extended with additional pathways, such as glycolysis or one-carbon metabolism, with the aim to perform *integrative modeling* of cell metabolism.

Finally, a key mechanism of the Ca^{2+} -mitochondria crosstalk and the metabolic efficiency management is the dynamical switch between SERCA and mitochondrial uptakes. Alterations in Ca^{2+} removal mechanisms due to mutations, generation of reactive oxygen species or remodeling of channel and pump expression are ubiquitous in pathological states such as mitochondrial (**Visch et al.,**

2006) and neurodegenerative diseases (Celsi *et al.*, 2009; Filadi and Pizzo, 2020), cancer (Monteith *et al.*, 2017) or diabetes (Guerrero-Hernandez and Verkhratsky, 2014), and therapeutic strategies targeting Ca^{2+} homeostasis and signaling have started to emerge (Giorgi *et al.*, 2012; Dejos *et al.*, 2020). Some of these changes can be captured by perturbations in the kinetic parameters of the Ca^{2+} fluxes (Soman *et al.*, 2017), which would make the use of our approach in the context of disease quite straightforward. Overall, our methodology thus paves the way for a more systematic characterization of the dynamical energetic impact of metabolism regulation, which could improve the current understanding of pathway selection mechanisms in health and disease.

Methods

Model development, methodology and calculations are detailed in the next sections as follows: (1) Description of the kinetic model, (2) Concepts of biothermodynamics and (3) Nonequilibrium thermodynamics analysis. A systematic description of the nonequilibrium thermodynamics of CRNs can be found in Rao and Esposito (2018) and Avanzini *et al.* (2021). This description can be applied to effective coarse-grained fluxes (Wachtel *et al.*, 2018; Avanzini *et al.*, 2020) such as the ones we used to characterize the enzyme-catalysed processes of our system. The chemical reactions incorporated in the model are listed in Table 1 and the corresponding fluxes and forces are given in Table 2 and Table 3, respectively. Lastly, the reference simulation parameters and a short description of their physical meaning can be found in Table 4. Simulation algorithms are publicly available at <https://gitlab.lcsb.uni.lu/ICS-lcsb/net-ca-mito.git> as of the date of publication. Transformed Gibbs free energies of reaction were retrieved from eQuilibrator (Flamholz *et al.*, 2012) and data were generated by running the simulation algorithms in Python (version 3.9.13).

Kinetic model

Mitochondrial reactions

Our model for mitochondrial metabolism is partly based on the pioneering work of Magnus and Keizer (Magnus and Keizer, 1997, 1998a,b). In particular, the synthesis of ATP by F1F0-ATPase and the oxidation of NADH into NAD^+ by the electron transport chain are both accompanied by a flux of protons across the mitochondrial membrane. While the reaction fluxes and the proton fluxes are described by slightly different expressions in the Magnus-Keizer model, we consider that the proton flux is a multiple of the reaction flux, and fix the proportionality coefficient according to the known stoichiometry (see Table 1), as done in previous models (Bertram *et al.*, 2006; Wacquier *et al.*, 2016). The Magnus-Keizer model accounts for mitochondrial carbon metabolism in a compact way, with effective fluxes for the TCA cycle and the associated generation of high energy electrons in the form of NADH. These fluxes have a constant component representing a basal flux, which is non-zero even in the absence of carbon input (glucose), and a contribution from glycolysis, which is assumed to be essentially captured by the flux through PDH (Magnus and Keizer, 1998a). Although these effective fluxes depend on $[\text{Ca}^{2+}]_m$ to account for the Ca^{2+} -regulation of PDH, they do not reflect the activatory role of Ca^{2+} on IDH and KGDH. We thus replace these effective contributions by incorporating the more detailed model of the TCA cycle from Dudycha *et al.* (Dudycha, 2000). A reaction current is associated to each of the 8 enzymatic reaction of the TCA cycles, which are subjected to possible regulations by Ca^{2+} , but also by Mg^{2+} , ATP, NADH, and others. Additionally, Dudycha's model accounts for the aspartate aminotransferase reaction, which is not part of the TCA cycle *per se*, but converts oxaloacetate and glutamate into α -ketoglutarate and aspartate. We neglect the aspartate aminotransferase reaction to focus exclusively on the TCA reactions. Finally, we use acetyl-CoA (AcCoA) at the entry of the TCA cycle as the carbon input of the mitochondrial metabolism instead of glucose at the entry of glycolysis like in Magnus-Keizer model. Note that these modifications are similar to the ones adopted by Cortassa *et al.* in Cortassa *et al.* (2003).

Cytosolic reactions and calcium signaling

In *Cortassa et al. (2003)*, $[\text{Ca}^{2+}]_c$ is as a constant parameter and the ATP-consuming Ca^{2+} exchanges between the endoplasmic reticulum (ER) and the cytosol are neglected. The resulting model can therefore not fully capture the crosstalk between mitochondrial ATP production and Ca^{2+} signaling. To close this gap, our model explicitly describes the coupling between ATP hydrolysis and the uptake of Ca^{2+} into the ER by SERCA pumps as done by *Wacquier et al. (Wacquier et al., 2016)*. More precisely, the SERCA flux is ATP-dependent and affects the cytosolic concentration of ATP. The Ca^{2+} uptake by SERCAs is balanced by the efflux of Ca^{2+} from the ER through IP_3 receptors (IP_3Rs) and passive leak through the membrane of the ER. The flux through IP_3Rs is modeled by a function depending solely on the concentrations of IP_3 and cytosolic Ca^{2+} , as in *Komin et al. (2015)*.

Fluxes and evolution equations

Overall, we consider 32 species and 17 chemical reactions taking place in or between compartments corresponding to the mitochondrial matrix, the cytosol and the ER. The chemical equations describing these reactions can be found in **Table 1**. A current J_κ (given in **Table 2**) is associated to each chemical reaction κ and is normalized with respect to the volume of the corresponding cell compartment (cytosol, ER or mitochondria). The concentration of the controlled species $\{\text{Pi}_c, \text{Pi}_m, \text{Na}_c^+, \text{Na}_m^+, \text{IP}_3, \text{H}_c^+, \text{H}_m^+, \text{O}_2, \text{H}_2\text{O}_c, \text{H}_2\text{O}_m, \text{AcCoA}, \text{CoA}, \text{CO}_2, \text{CoQH}_2, \text{CoQ}\}$ is fixed in time (see also **Figure 1** in the main text), meaning that the effect of chemical reactions is balanced by additional processes which are not described explicitly in the model. The rate equations for the other species are given in **Equation 6–Equation 23**. Stoichiometric and volumetric coefficients are included in **Equation 6–Equation 23** to guarantee mass balance across cell compartments. Specifically, $\alpha = V_{\text{ER}}/V_c$ and $\delta = V_m/V_c$, where V_c , V_{ER} and V_m are the volumes of the cytosol, of the ER and of mitochondria, respectively. Ca^{2+} buffering in these compartments is accounted for by the coefficients f_c , f_{ER} and f_m , which correspond to the fraction of free Ca^{2+} in the compartment of interest. Finally, we mention that all fluxes are expressed in mM/s and concentration units are mM, except for Ca^{2+} concentrations which are in μM , and coefficient $\gamma = 10^3 \mu\text{M}/\text{mM}$ is therefore introduced to ensure consistency in units.

$$d_t [\text{ADP}]_c = -\delta J_{\text{ANT}} + J_{\text{Hyd}} + \frac{1}{2} J_{\text{SERCA}} \quad (6)$$

$$d_t [\text{ADP}]_m = J_{\text{ANT}} - J_{\text{F}_1} - J_{\text{SL}} \quad (7)$$

$$d_t [\alpha\text{KG}]_m = J_{\text{IDH}} - J_{\text{KGDH}} \quad (8)$$

$$d_t [\text{ATP}]_c = \delta J_{\text{ANT}} - J_{\text{Hyd}} - \frac{1}{2} J_{\text{SERCA}} \quad (9)$$

$$d_t [\text{ATP}]_m = -J_{\text{ANT}} + J_{\text{F}_1} + J_{\text{SL}} \quad (10)$$

$$d_t [\text{Ca}^{2+}]_c = \frac{f_c}{\gamma} (-J_{\text{SERCA}} + J_{\text{ERout}} + \delta (J_{\text{NCX}} - J_{\text{UNI}})) \quad (11)$$

$$d_t [\text{Ca}^{2+}]_m = \frac{f_m}{\gamma} (J_{\text{UNI}} - J_{\text{NCX}}) \quad (12)$$

$$d_t [\text{Ca}^{2+}]_{\text{ER}} = -\frac{f_{\text{ER}}}{\gamma\alpha} (J_{\text{SERCA}} - J_{\text{ERout}}) \quad (13)$$

$$d_t [\text{CIT}]_m = J_{\text{CS}} - J_{\text{ACO}} \quad (14)$$

$$d_t [\text{FUM}]_m = J_{\text{SDH}} - J_{\text{FH}} \quad (15)$$

$$d_t [\text{ISOC}]_m = J_{\text{ACO}} - J_{\text{IDH}} \quad (16)$$

$$d_t [\text{MAL}]_m = J_{\text{FH}} - J_{\text{MDH}} \quad (17)$$

$$d_t [\text{NAD}]_m = J_{\text{Ox}} - J_{\text{IDH}} - J_{\text{KGDH}} - J_{\text{MDH}} \quad (18)$$

$$d_t [\text{NADH}]_m = -J_{\text{Ox}} + J_{\text{IDH}} + J_{\text{KGDH}} + J_{\text{MDH}} \quad (19)$$

$$d_t [\text{OAA}]_m = J_{\text{MDH}} - J_{\text{CS}} \quad (20)$$

$$d_t \Delta\Psi = \frac{1}{c_m} (10 J_{\text{Ox}} - 3 J_{\text{F}_1} - J_{\text{ANT}} - J_{\text{HI}} - J_{\text{NCX}} - 2 J_{\text{UNI}}) \quad (21)$$

$$d_t [\text{SCoA}]_m = J_{\text{KGDH}} - J_{\text{SL}} \quad (22)$$

$$d_t [\text{SUC}]_m = J_{\text{SL}} - J_{\text{SDH}} \quad (23)$$

Concepts of biothermodynamics

Definitions

The entropy production rate (EPR) associated to a chemical reaction ρ is given by

$$\sigma_\rho = -\frac{J_\rho \Delta_r G_\rho}{T} \geq 0, \quad (24)$$

where T is the absolute temperature while J_ρ and $\Delta_r G_\rho$ are the current and Gibbs free energy of reaction ρ , respectively. In nonequilibrium thermodynamics, $-\Delta_r G_\rho$ is the *force* driving the reaction while J_ρ is the reaction *flux* resulting from this force. The equilibrium state is characterized by zero forces and hence zero fluxes.

The Gibbs free energy of reaction ρ is defined by (*De Groot and Mazur, 1984*)

$$\Delta_r G_\rho = \sum_i \mathbb{S}_i^\rho \mu_i, \quad (25)$$

where \mathbb{S}_i^ρ is the net stoichiometric coefficient of species i in reaction ρ and μ_i is the chemical potential of species i . Under the hypothesis of *local equilibrium*, i.e., state variables such as temperature and pressure relax to equilibrium on a much faster timescale than chemical reactions, the expressions for the chemical potentials derived at equilibrium still hold locally out-of-equilibrium (*De Groot and Mazur, 1984*). The chemical potential μ_i is thus given by

$$\mu_i = \mu_i^\circ + RT \ln a_i, \quad (26)$$

where μ_i° and a_i denote the standard chemical potential and the activity of species i , respectively. The activity accounts for the interactions between chemical species present in solution and is related to the concentration by the coefficient of activity γ_i , which depends on the ionic strength (*Alberty, 2003*), I , such that $a_i = \gamma_i \frac{[i]}{c^\circ}$, where $[i]$ and c° are the concentration of species i and standard concentration, respectively. In ideal solutions, $\gamma_i = 1$. Standard conditions correspond to atmospheric pressure $p^\circ = 1$ bar and molar concentrations $c^\circ = 1$ M.

Standard chemical potentials are directly related to the standard Gibbs free energy of reaction $\Delta_r G_\rho^\circ = \sum_i \mathbb{S}_i^\rho \mu_i^\circ = -RT \ln K_\rho$, where $K_\rho = \prod_i a_{i,eq}^{\mathbb{S}_i^\rho}$ is the equilibrium constant of reaction ρ . Hence, $\Delta_r G_\rho$ can then be rewritten as

$$\Delta_r G_\rho = \Delta_r G_\rho^\circ + RT \ln \prod_i a_i^{\mathbb{S}_i^\rho} = RT \ln \prod_i \left(\frac{a_i}{a_{i,eq}} \right)^{\mathbb{S}_i^\rho}. \quad (27)$$

From a practical point of view, standard Gibbs free energies of reaction and activity coefficients are usually available in thermodynamic tables. As described in the next subsection, further adaptations can be done to describe more adequately the physiological environment in which biochemical reactions take place.

Physiological conditions

Cells are compartmentalized into specialized organelles whose composition can widely differ. For example, mitochondrial and cytosolic pH are 8 (*Casey et al., 2010*) and 7.2 (*Buckler and Vaughan-Jones, 1990*), respectively. A plethora of buffering mechanisms regulate their internal concentration of metallic ions and pH, and thereby ensures the maintenance of homeostasis. Some chemical species can exist in different forms, that is, bound to metallic cations or at different levels of protonation (for example, "ATP" can be ATP^{4-} , HATP^{3-} , MgATP^{2-} , etc.), and their relative abundance depends on the internal environment of the organelle. For the sake of compactness, biochemical reactions are thus usually written in terms of *pseudoisomers*, that is, without explicitly mentioning the state of the species and without detailing the consumption or production of protons/metallic ions by the reaction (e.g. $\text{ATP} + \text{H}_2\text{O} \rightleftharpoons \text{ADP} + \text{P}_i$) (*Alberly, 2003*).

To describe biochemical reactions from a thermodynamic point of view, their associated standard Gibbs free energy can be rescaled to match the equilibrium corresponding the physiological pH and metallic ions concentrations, but also incorporates the activity coefficients corresponding to a physiological ionic strength ($I = 0.120 \text{ M}$ (*Alberly, 2003; Robinson et al., 2006*)). The resulting $\Delta_r G'_\kappa$ is subsequently used to calculate the transformed Gibbs free energy of reaction

$$\Delta_r G'_\kappa = \Delta_r G'_\kappa{}^\circ + RT \ln \prod_j [j]^{\mathbb{S}_j^\kappa}, \quad (28)$$

where $[j]$ is the concentration of pseudoisomer j and \mathbb{S}_j^κ is the net stoichiometric coefficient of pseudoisomer j in reaction κ . Complementary approaches (*Noor et al., 2012, 2013b*) have led to the development of databases (*Goldberg et al., 2004; Flamholz et al., 2012*) from which we retrieved $\Delta_r G'_\kappa$ for different pH, ionic strength and metallic ion concentrations.

Electrogenic processes, such as Ca^{2+} exchanges, the exchange of ATP^{4-} and ADP^{3-} *via* the antiporter and the transfer of protons accompanying oxidative phosphorylation, constitute notable exceptions where the charges of species need to be explicitly accounted for. Indeed, electrostatic interactions affect the Gibbs free energy and in that case, the right-hand side of Eq. 28 must also comprise the term related to the electric potential in the compartment of interest. We thus distinguish the charged species $\{i\}$ from the pseudoisomers $\{j\}$. More precisely, $\Delta_r G'_\kappa = \sum_j \mathbb{S}_j^\kappa \mu_j + \sum_i \mathbb{S}_i^\kappa \bar{\mu}_i$ where $\bar{\mu}_i$ is the *electrochemical potential*

$$\bar{\mu}_i = \mu_i^\circ + RT \ln a_i + z_i F V_{r(i)}, \quad (29)$$

where z_i is the charge of species i (for example, $z = +2$ for Ca^{2+}), F is the Faraday constant and $V_{r(i)}$ is the electric potential in the compartment r where species i is considered. Overall, this leads to

$$\Delta_r G'_\kappa = \Delta_r G'_\kappa{}^\circ + RT \ln \prod_j [j]^{\mathbb{S}_j^\kappa} + RT \ln \prod_i [i]^{\mathbb{S}_i^\kappa} + \sum_i \mathbb{S}_i^\kappa z_i F V_{r(i)}. \quad (30)$$

When a charged species is exchanged between two compartments, the $\Delta_r G'_\kappa$ associated to this transport process depends on the difference of potential between the two compartments. For

example, if we consider the transport of Ca^{2+} from cytosol to mitochondria, $\Delta_r G'_k = RT \ln \frac{[\text{Ca}^{2+}]_m}{[\text{Ca}^{2+}]_c} + 2F(V_m - V_c) = RT \ln \frac{[\text{Ca}^{2+}]_m}{[\text{Ca}^{2+}]_c} - 2F\Delta\psi$.

Although pH (and hence proton concentrations) in mitochondria and cytosol are assumed to be constant due to strong buffering, proton transfer across mitochondrial membrane still affects the membrane potential (at least, at the local scale that is considered in the present model), which in turns affect $\Delta_r G'_k$. The expressions for the $\Delta_r G'_k$ of each process of the model can be found in **Table 3**.

Nonequilibrium thermodynamic analysis

Mitochondria as chemical engines

Mitochondria can be considered as engines converting ADP_c into ATP_c via 11 so-called *internal reactions*

$$\kappa_i \in \{\text{ANT, F1, OX, CS, ACO, IDH, KGDH, SL, SDH, FH, MDH}\},$$

modeling mitochondrial metabolism, which are coupled to 6 *external reactions*

$$\kappa_e \in \{\text{ERout, SERCA, NCX, UNI, HYD, HI}\},$$

representing Ca^{2+} signaling, cell activity and ionic homeostasis. The chemical species involved in internal reactions are categorized into two groups, referred to as *internal species*

$$X \in \{\text{ATP}_m, \text{ADP}_m, \text{NADH, NAD, OAA, CIT, ISOC, } \alpha\text{KG, SCoA, SUC, FUM, MAL}\},$$

and *exchanged species*

$$Y \in \{\text{ATP}_c, \text{ADP}_c, \text{Pi}_m, \text{H}_c^+, \text{H}_m^+, \text{O}_2, \text{H}_2\text{O}_m, \text{AcCoA, CoA, CO}_2, \text{CoQ, CoQH}_2\}.$$

The former is the set of species involved only in the internal reactions, while the latter includes the controlled species and the species involved also in the external reactions. Thus, the rate equations for internal and exchanged species can be respectively written as

$$d_t [X] = \sum_{\kappa_i} \mathbb{S}_{\kappa_i}^X J_{\kappa_i}, \quad (31a)$$

$$\frac{V_{\text{ref}}^Y}{V_m} d_t [Y] = \sum_{\kappa_i} \mathbb{S}_{\kappa_i}^Y J_{\kappa_i} + I^Y, \quad (31b)$$

where V_{ref}^Y is the volume of the compartment to which species Y belongs, and I^Y is the exchange current either accounting for the external reactions (named flux control in **Avanzini and Esposito (2022)**) or modeling additional processes that are responsible for the homeostasis of the controlled species (named concentration control in **Avanzini and Esposito (2022)**). On the one hand ATP_c and ADP_c are involved in the external reactions SERCA and HYD and hence $I^{\text{ATP}_c} = -I^{\text{ADP}_c} = \frac{1}{\delta}(-\frac{1}{2}J_{\text{SERCA}} - J_{\text{HYD}})$; on the other hand, the other exchanged species (*i.e.*, $\text{Pi}_m, \text{H}_m^+, \text{H}_c^+, \text{O}_2, \text{H}_2\text{O}_m, \text{AcCoA, CoA, CO}_2, \text{CoQH}_2, \text{CoQ}$) are controlled species and hence $I^Y = -\sum_{\kappa_i} \mathbb{S}_{\kappa_i}^Y J_{\kappa_i}$.

Second law for mitochondrial metabolism

In general, the second law of thermodynamics for open CRNs can be written as (**Rao and Esposito, 2018; Avanzini et al., 2021**)

$$T\sigma = -d_t \mathcal{G} + \dot{w}_{\text{nc}} + \dot{w}_{\text{driv}}, \quad (32)$$

where \mathcal{G} is the (semi-grand) *Gibbs free energy* of the system, while \dot{w}_{nc} and \dot{w}_{driv} , respectively referred to as the *nonconservative work rate* and the *driving work rate*, are related to the energetic cost of maintaining CRNs out of equilibrium via the exchange of species $\{Y\}$. Since \mathcal{G} is a state function, its time derivative vanishes at steady state as well as when averaged over one period in the case of an oscillatory regime.

In the following, we use the topological analysis developed in *Rao and Esposito (2018); Avanzini et al. (2021)* to derive the explicit expressions of the nonconservative work rate and the driving work rate for mitochondrial metabolism.

Remark: The rate equations (*Equation 6-Equation 23*) are coarse-grained, namely, each reactive process represents a sequence of out-of-equilibrium elementary reactions involving intermediate species whose dynamical behavior is not described. Each of these elementary reactions might affect the energetics of the whole system. Nevertheless, under the assumption of the existence of a time scale separation between the evolution of the species accounted by the dynamical model and the coarse-grained intermediate species, our thermodynamic analysis characterizes the correct energetics of the whole system as proven in *Avanzini et al. (2020, 2023)*.

Conservation laws and emergent cycles

For our model, the *stoichiometric matrix* \mathbb{S} encoding the net stoichiometric coefficients of internal species X and exchanged species Y in the internal reactions κ_i reads

$$\mathbb{S} = \begin{array}{c} \begin{array}{l} \text{ATP}_m \\ \text{ADP}_m \\ \text{NADH} \\ \text{NAD} \\ \text{OAA} \\ \text{CIT} \\ \text{ISOC} \\ \alpha\text{KG} \\ \text{SCoA} \\ \text{SUC} \\ \text{FUM} \\ \text{MAL} \\ \text{ADP}_c \\ \text{P}_m^+ \\ \text{H}_m^+ \\ \text{O}_2 \\ \text{H}_2\text{O}_m \\ \text{AcCoA} \\ \text{CoA} \\ \text{CO}_2 \\ \text{CoQH}_2 \\ \text{CoQ} \\ \text{ATP}_c \\ \text{H}_c^+ \end{array} \begin{array}{c} \left(\begin{array}{cccccccccccc} \text{ANT} & \text{F1} & \text{OX} & \text{CS} & \text{ACO} & \text{IDH} & \text{KGDH} & \text{SL} & \text{SDH} & \text{FH} & \text{MDH} \\ -1 & 1 & 0 & 0 & 0 & 0 & 0 & 1 & 0 & 0 & 0 \\ 1 & -1 & 0 & 0 & 0 & 0 & 0 & -1 & 0 & 0 & 0 \\ 0 & 0 & -1 & 0 & 0 & 1 & 1 & 0 & 0 & 0 & 1 \\ 0 & 0 & 1 & 0 & 0 & -1 & -1 & 0 & 0 & 0 & -1 \\ 0 & 0 & 0 & -1 & 0 & 0 & 0 & 0 & 0 & 0 & 1 \\ 0 & 0 & 0 & 1 & -1 & 0 & 0 & 0 & 0 & 0 & 0 \\ 0 & 0 & 0 & 0 & 1 & -1 & 0 & 0 & 0 & 0 & 0 \\ 0 & 0 & 0 & 0 & 0 & 1 & -1 & 0 & 0 & 0 & 0 \\ 0 & 0 & 0 & 0 & 0 & 0 & 0 & 1 & -1 & 0 & 0 \\ 0 & 0 & 0 & 0 & 0 & 0 & 0 & 0 & 1 & -1 & 0 \\ 0 & 0 & 0 & 0 & 0 & 0 & 0 & 0 & 0 & 1 & -1 \\ -1 & 0 & 0 & 0 & 0 & 0 & 0 & 0 & 0 & 0 & 0 \\ 0 & -1 & 0 & 0 & 0 & 0 & 0 & -1 & 0 & 0 & 0 \\ 0 & 3 & -10 & 0 & 0 & 0 & 0 & 0 & 0 & 0 & 0 \\ 0 & 0 & -\frac{1}{2} & 0 & 0 & 0 & 0 & 0 & 0 & 0 & 0 \\ 0 & 1 & 1 & -1 & 0 & 0 & 0 & 0 & 0 & -1 & 0 \\ 0 & 0 & 0 & -1 & 0 & 0 & 0 & 0 & 0 & 0 & 0 \\ 0 & 0 & 0 & 1 & 0 & 0 & -1 & 1 & 0 & 0 & 0 \\ 0 & 0 & 0 & 0 & 0 & 1 & 1 & 0 & 0 & 0 & 0 \\ 0 & 0 & 0 & 0 & 0 & 0 & 0 & 0 & 1 & 0 & 0 \\ 0 & 0 & 0 & 0 & 0 & 0 & 0 & 0 & -1 & 0 & 0 \\ 1 & 0 & 0 & 0 & 0 & 0 & 0 & 0 & 0 & 0 & 0 \\ 0 & -3 & 10 & 0 & 0 & 0 & 0 & 0 & 0 & 0 & 0 \end{array} \right) \end{array} \end{array} \quad (33)$$

The 13 (linearly-independent) left-null eigenvectors of \mathbb{S} , encoded as rows of the matrix

$$\mathbb{L} = \begin{matrix} & \text{ATP}_m & \text{ADP}_m & \text{NADH} & \text{NAD} & \text{OAA} & \text{CIT} & \text{ISOC} & \alpha\text{KG} & \text{SCoA} & \text{SUC} & \text{FUM} & \text{MAL} & \text{ADP}_c & \text{Pi}_m & \text{H}_m^+ & \text{O}_2 & \text{H}_2\text{O}_m & \text{AcCoA} & \text{CoA} & \text{CO}_2 & \text{CoQH}_2 & \text{CoQ} & \text{ATP}_c & \text{H}_c^+ \\ \text{H}_m^+ & \left(\begin{array}{c|c} 0 & 0 & 0 & 0 & 0 & 0 & 0 & 0 & 0 & 0 & 0 & 0 & 0 & 0 & 0 & 1 & 0 & 0 & 0 & 0 & 0 & 0 & 0 & 0 & 0 & 1 \\ 0 & 0 & 0 & 0 & 0 & 0 & 0 & 0 & 0 & 0 & 0 & 0 & 0 & 1 & 0 & 0 & 0 & 0 & 0 & 0 & 0 & 0 & 0 & 0 & 1 & 0 \\ 3 & 0 & 10 & 0 & -10 & -10 & -10 & -20 & -30 & -33 & 0 & 0 & -3 & 0 & -1 & 0 & 0 & 0 & 0 & 0 & 0 & 0 & 33 & 0 & 0 & 0 \\ -3 & 0 & -10 & 0 & 10 & 10 & 10 & 20 & 30 & 33 & 0 & 0 & 3 & 0 & 1 & 0 & 0 & 0 & 0 & 0 & 0 & 33 & 0 & 0 & 0 & 0 \\ -6 & 0 & -20 & 0 & 20 & 20 & 20 & 7 & -6 & 0 & 0 & 0 & 6 & 0 & 2 & 0 & 0 & 0 & 0 & 33 & 0 & 0 & 0 & 0 & 0 & 0 \\ -3 & 0 & -10 & 0 & 10 & -23 & -23 & -13 & 30 & 0 & 0 & 0 & 3 & 0 & 1 & 0 & 0 & 0 & 33 & 0 & 0 & 0 & 0 & 0 & 0 & 0 \\ 3 & 0 & 10 & 0 & -10 & 23 & 23 & 13 & 3 & 0 & 0 & 0 & -3 & 0 & -1 & 0 & 0 & 33 & 0 & 0 & 0 & 0 & 0 & 0 & 0 & 0 \\ -1 & 0 & 1 & 0 & -1 & 0 & 0 & -1 & -2 & -1 & -1 & 0 & 1 & 0 & 0 & 0 & 1 & 0 & 0 & 0 & 0 & 0 & 0 & 0 & 0 & 0 \\ 3 & 0 & -1 & 0 & 1 & 1 & 1 & 2 & 3 & 0 & 0 & 0 & -3 & 0 & -1 & 22 & 0 & 0 & 0 & 0 & 0 & 0 & 0 & 0 & 0 & 0 \\ 1 & 0 & 0 & 0 & 0 & 0 & 0 & 0 & 0 & 0 & 0 & 0 & -1 & 1 & 0 & 0 & 0 & 0 & 0 & 0 & 0 & 0 & 0 & 0 & 0 & 0 \\ \hline 0 & 0 & 0 & 0 & 1 & 1 & 1 & 1 & 1 & 1 & 1 & 1 & 1 & 0 & 0 & 0 & 0 & 0 & 0 & 0 & 0 & 0 & 0 & 0 & 0 & 0 & 0 \\ 0 & 0 & 1 & 1 & 0 \\ 1 & 1 & 0 \end{array} \right. \end{matrix}, \quad (34)$$

which therefore satisfies $\mathbb{L}\mathbb{S} = 0$, define the conservation laws. Indeed, for the every row λ of \mathbb{L} (labeled using chemical symbols in [Equation 34](#) for reasons that will be explained in subsection Potential and force species), the quantity $L^\lambda = \sum_X \mathbb{L}_X^\lambda [X] + \sum_Y \mathbb{L}_Y^\lambda [Y]$ would be a conserved quantity if mitochondria were closed systems, namely, if $I^Y = 0 \forall Y$. When $I^Y \neq 0$, only 3 out of the 13 conservation laws corresponding to the last three rows of \mathbb{L} in [Equation 34](#) involve exclusively internal species and their corresponding quantities $L^\lambda = \sum_X \mathbb{L}_X^\lambda [X]$ are still conserved. These conservation laws are said to be *unbroken*. The other conservation laws correspond to quantities $L^\lambda = \sum_X \mathbb{L}_X^\lambda [X] + \sum_Y \mathbb{L}_Y^\lambda [Y]$ that are not conserved anymore and are, therefore, named *broken* conservation laws.

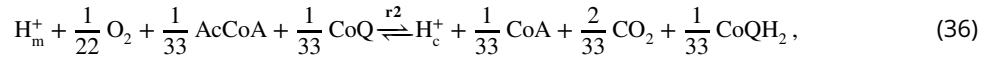
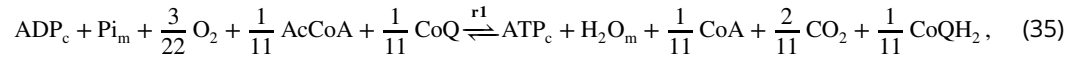
The 2 (linearly-independent) right-null eigenvectors of \mathbb{S}^X (*i.e.*, the (sub)stoichiometric matrix for the internal species),

$$\mathbf{c}_{r1} = \left(\begin{array}{c|c} \text{ANT} & \text{F1} & \text{OX} & \text{CS} & \text{ACO} & \text{IDH} & \text{KGDH} & \text{SL} & \text{SDH} & \text{FH} & \text{MDH} \\ 1 & \frac{10}{11} & \frac{3}{11} & \frac{1}{11} & \frac{1}{11} & \frac{1}{11} & \frac{1}{11} & \frac{1}{11} & \frac{1}{11} & \frac{1}{11} & \frac{1}{11} \end{array} \right),$$

and

$$\mathbf{c}_{r2} = \left(\begin{array}{c|c} \text{ANT} & \text{F1} & \text{OX} & \text{CS} & \text{ACO} & \text{IDH} & \text{KGDH} & \text{SL} & \text{SDH} & \text{FH} & \text{MDH} \\ 0 & -\frac{1}{33} & \frac{1}{11} & \frac{1}{33} & \frac{1}{33} & \frac{1}{33} & \frac{1}{33} & \frac{1}{33} & \frac{1}{33} & \frac{1}{33} & \frac{1}{33} \end{array} \right),$$

are named *emergent cycles*. They define sequences of reactions that overall leave the abundances of the internal species unchanged, since $\mathbb{S}^X \mathbf{c}_{r1} = 0$ and $\mathbb{S}^X \mathbf{c}_{r2} = 0$ by definition, while interconverting the exchanged species as they undergo the effective reactions



whose stoichiometry is defined by $\mathbb{S}^Y \mathbf{c}_{r1}$ and $\mathbb{S}^Y \mathbf{c}_{r2}$, respectively, with \mathbb{S}^Y the (sub)stoichiometric matrix for the exchanged species.

Potential and force species

The exchanged species $\{Y\}$ can be classified as either *potential* species $\{Y_p\}$ or as *force* species $\{Y_f\}$. The potential species are the largest subset of exchanged species such that the submatrix $\mathbb{L}_{Y_p}^b$ of \mathbb{L} for the broken conservation laws and the potential species can be inverted, *i.e.*, $(\mathbb{L}_{Y_p}^b)^{-1}$ exists. The force species are the remaining species $\{Y_f\} = \{Y\} \setminus \{Y_p\}$. As discussed in [Rao and Esposito \(2018\)](#); [Avanzini et al. \(2021\)](#), this partitioning is not unique, but different choices do not change the conclusions of the thermodynamic analysis.

In our model, we choose

$$Y_p \in \{\text{ADP}_c, \text{Pi}_m, \text{H}_m^+, \text{O}_2, \text{H}_2\text{O}_m, \text{AcCoA}, \text{CoA}, \text{CO}_2, \text{CoQ}, \text{CoQH}_2\}$$

and

$$Y_f \in \{\text{ATP}_c, \text{H}_c^+\}.$$

In Eq. 33, the horizontal lines split \mathbb{S} into

$$\mathbb{S} = \begin{pmatrix} \mathbb{S}^X \\ \mathbb{S}^{Y_p} \\ \mathbb{S}^{Y_f} \end{pmatrix} \quad (37)$$

In Eq. 34 the horizontal and vertical lines split \mathbb{L} into

$$\mathbb{L} = \begin{pmatrix} \mathbb{L}_X^b & | & \mathbb{L}_{Y_p}^b & | & \mathbb{L}_{Y_f}^b \\ \hline \mathbb{L}_X^u & | & \mathbb{L}_{Y_p}^u & | & \mathbb{L}_{Y_f}^u \end{pmatrix} \quad (38)$$

with u and b for unbroken and broken conservation laws, respectively.

Note that the existence of $(\mathbb{L}_{Y_p}^b)^{-1}$ defines a representation of the broken conservation laws given by $(\mathbb{L}_{Y_p}^b)^{-1}\mathbb{L}^b$ where every broken conservation law involves only one potential species. This physically means that each quantity L^λ corresponding to a broken conservation law stops being conserved once a specific potential species is exchanged. Furthermore, no new quantities L^λ stop being conserved when the force species are exchanged. For this reason, each conservation law λ in **Equation 34** can always be labeled using the chemical symbol of the potential species that, once exchanged, would make L^λ a nonconserved quantity.

Nonconservative work

The general expression of the nonconservative work rate is given by

$$\dot{w}_{nc} = \mathcal{F}_{Y_f} \cdot \mathbf{I}^{Y_f} \quad (39)$$

where

$$\mathcal{F}_{Y_f} = (\boldsymbol{\mu}_{Y_f} \cdot \mathbb{L} - \boldsymbol{\mu}_{Y_p} \cdot (\mathbb{L}_{Y_p}^b)^{-1} \mathbb{L}_{Y_f}^b)^\top \quad (40)$$

is the vector of the nonconservative forces, \mathbf{I}^{Y_f} is the vector collecting the exchange currents of the force species, and $\boldsymbol{\mu}_{Y_f}$ (resp. $\boldsymbol{\mu}_{Y_p}$) is the vector of the chemical/electrochemical potential of the force (resp. potential) species.

In our model, there are only two force species, namely, ATP_c and H_c^+ . The two corresponding nonconservative forces are given by

$$\mathcal{F}_{\text{ATP}_c} = -\frac{\mu_{\text{AcCoa}}}{11} - \mu_{\text{ADP}_c} + \mu_{\text{ATP}_c} + \frac{2\mu_{\text{CO}_2}}{11} + \frac{\mu_{\text{CoA}}}{11} - \frac{\mu_{\text{CoQ}}}{11} + \frac{\mu_{\text{CoQH}_2}}{11} + \mu_{\text{H}_2\text{O}_m} - \frac{3\mu_{\text{O}_2}}{22} - \mu_{\text{Pim}} \quad (41)$$

and

$$\mathcal{F}_{\text{H}_c^+} = -\frac{\mu_{\text{AcCoa}}}{33} + \frac{2\mu_{\text{CO}_2}}{33} + \frac{\mu_{\text{CoA}}}{33} - \frac{\mu_{\text{CoQ}}}{33} + \frac{\mu_{\text{CoQH}_2}}{33} + \mu_{\text{H}_c} - \mu_{\text{H}_m} - \frac{\mu_{\text{O}_2}}{22} \quad (42)$$

while the exchange currents are

$$I^{\text{ATP}_c} = \frac{1}{\delta} \left(-J_{\text{Hyd}} - \frac{1}{2} J_{\text{SERCA}} \right), \quad (43)$$

and

$$I^{\text{H}_c^+} = 3 J_{\text{F}_1} - 10 J_{\text{O}_X}. \quad (44)$$

Equation 43 is obtained by writing the rate equation for ATP_c (**Equation 9**) according to **Equation 31b**: $\frac{1}{\delta} d_t [\text{ATP}]_c = J_{\text{ANT}} + I^{\text{ATP}_c}$. **Equation 44** is obtained by recognising that H_c^+ is a controlled species, *i.e.*, $d_t [\text{H}^+]_c = 0$, and using again **Equation 31b**, we can write $\frac{1}{\delta} d_t [\text{H}^+]_c = 0 = 10 J_{\text{O}_X} - 3 J_{\text{F}_1} + I^{\text{H}_c^+}$.

Notice that the nonconservative forces in **Equation 41** and **Equation 42** correspond exactly to $\Delta_r G'_{r1}$ and $\Delta_r G'_{r2}$ of the effective reactions in **Equation 35** and **Equation 36**. They can therefore be rewritten as

$$\mathcal{F}_{\text{ATP}_c} = \Delta_r G'_{\text{ANT}} + \frac{10 \Delta_r G'_{\text{F}_1}}{11} + \frac{3 \Delta_r G'_{\text{O}_X}}{11} + \frac{\Delta_r G'_{\text{TCA}}}{11} = \Delta_r G'_{r1} \quad (45)$$

and

$$\mathcal{F}_{\text{H}^+} = -\frac{\Delta_r G'_{\text{F1}}}{33} + \frac{\Delta_r G'_{\text{OX}}}{11} + \frac{\Delta_r G'_{\text{TCA}}}{33} = \Delta_r G'_{r2} \quad (46)$$

where $\Delta_r G'_{\text{TCA}} := \Delta_r G'_{\text{CS}} + \Delta_r G'_{\text{ACO}} + \Delta_r G'_{\text{IDH}} + \Delta_r G'_{\text{KGDH}} + \Delta_r G'_{\text{SL}} + \Delta_r G'_{\text{SDH}} + \Delta_r G'_{\text{FH}} + \Delta_r G'_{\text{MDH}}$. We numerically compute the nonconservative forces using the latter expressions. The expression of the nonconservative work rate for our model then becomes

$$\dot{w}_{\text{nc}} = \Delta_r G'_{r1} I^{\text{ATPc}} + \Delta_r G'_{r2} I^{\text{H}^+}. \quad (47)$$

Driving work

The driving work rate is in general given by the sum of two contributions,

$$\dot{w}_{\text{driv}} = \dot{w}_{\text{driv}}^{\text{ch}} + \dot{w}_{\text{driv}}^{\text{in}}, \quad (48)$$

namely, the *chemical driving work rate*

$$\dot{w}_{\text{driv}}^{\text{ch}} = -\left(\mathbf{d}_t \boldsymbol{\mu}_{Y_p}\right) \cdot \left(\mathbb{L}_{Y_p}^b\right)^{-1} \mathbb{L}^b [\mathbf{Z}], \quad (49)$$

and the *interaction driving work rate*

$$\dot{w}_{\text{driv}}^{\text{in}} = \nabla_{[e]} G^{\text{in}}([\mathbf{Z}], [e]) \cdot \mathbf{d}_t [e], \quad (50)$$

Here, $[\mathbf{Z}] = ([\mathbf{X}], [\mathbf{Y}])$ is a vector collecting the concentrations of both internal and exchanged species, $[e]$ is a vector collecting the concentrations of other interacting species (*i.e.*, Na_m^+ , Ca_m^{2+}) that are not interconverted by the internal reactions and that do not appear in \mathbb{S} , $\nabla_{[e]}$ is the gradient with respect to $[e]$ and $G^{\text{in}}([\mathbf{Z}], [e])$ is the interaction Gibbs free energy, whose exact expression depends on the model used to describe interactions (*Avanzini et al., 2021*).

In our model, we compute the driving work rate over one period t_p in the oscillatory regime (as it vanishes at steady state). The specific expression of the average chemical driving work rate is given by

$$\begin{aligned} \frac{1}{t_p} \int_0^{t_p} dt \dot{w}_{\text{driv}}^{\text{ch}} = & \frac{1}{t_p} \int_0^{t_p} dt \left(-\mathbf{d}_t \mu_{\text{ADPc}} L^{\text{ADPc}} - \mathbf{d}_t \mu_{\text{Pim}} L^{\text{Pim}} - \mathbf{d}_t \mu_{\text{Hm}^+} L^{\text{Hm}^+} - \mathbf{d}_t \mu_{\text{O}_2} L^{\text{O}_2}/22 - \mathbf{d}_t \mu_{\text{H}_2\text{O}} L^{\text{H}_2\text{O}} \right. \\ & \left. - \mathbf{d}_t \mu_{\text{AcCoA}} L^{\text{AcCoA}}/33 - \mathbf{d}_t \mu_{\text{CoA}} L^{\text{CoA}}/33 - \mathbf{d}_t \mu_{\text{CO}_2} L^{\text{CO}_2}/33 - \mathbf{d}_t \mu_{\text{CoQH}_2} L^{\text{CoQH}_2}/33 - \mathbf{d}_t \mu_{\text{CoQ}} L^{\text{CoQ}}/33 \right). \end{aligned} \quad (51)$$

Notice that the terms corresponding to uncharged controlled species (*i.e.*, Pim , O_2 , H_2O_m , AcCoA , CoA , CO_2 , CoQH_2 , CoQ) vanish since their chemical potential is constant over time. For the charged controlled species H_m^+ , the quantity L^{Hm^+} is still conserved since $[\text{H}^+]_m$ and $[\text{H}^+]_c$ are constant. Hence,

$$\begin{aligned} \frac{1}{t_p} \int_0^{t_p} dt \left(\mathbf{d}_t \mu_{\text{Hm}^+} L^{\text{Hm}^+} \right) = & \frac{L^{\text{Hm}^+}}{t_p} \int_0^{t_p} dt \left(\mathbf{d}_t \mu_{\text{Hm}^+} \right) = 0 \text{ since the electrochemical potential is a state function.} \\ \text{Similarly, } L^{\text{ADPc}} = & [\text{ADP}]_c + [\text{ATP}]_c \text{ is still conserved in the open system implying } \frac{1}{t_p} \int_0^{t_p} dt \left(-\mathbf{d}_t \mu_{\text{ADPc}} L^{\text{ADPc}} \right) = \\ \frac{L^{\text{ADPc}}}{t_p} \int_0^{t_p} dt \left(-\mathbf{d}_t \mu_{\text{ADPc}} \right) = & 0. \text{ In conclusion, the chemical driving work rate over one period vanishes:} \end{aligned}$$

$$\frac{1}{t_p} \int_0^{t_p} dt \dot{w}_{\text{driv}}^{\text{ch}} = 0. \quad (52)$$

We cannot determine the explicit expression of the interacting driving work rate since our model does not provide the interaction Gibbs free energy $G^{\text{in}}([\mathbf{Z}], [e])$. Thus, we compute the driving work over one period by calculating the total entropy production rate as the sum of the individual EPR of each internal reaction $\kappa_i = \{\text{ANT}, \text{F1}, \text{OX}, \text{CS}, \text{ACO}, \text{IDH}, \text{KGDH}, \text{SL}, \text{SDH}, \text{FH}, \text{MDH}\}$,

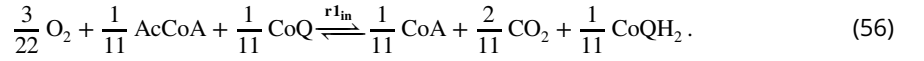
$$T\sigma = -\sum_{\kappa_i} \Delta_r G'_{\kappa_i} J_{\kappa_i} \quad (53)$$

from which we subtract the nonconservative work over one period:

$$\frac{1}{t_p} \int_0^{t_p} dt \dot{w}_{\text{driv}} = \frac{1}{t_p} \int_0^{t_p} dt (T\sigma - \dot{w}_{\text{nc}}). \quad (54)$$

Thermodynamic efficiency

In subsection *Second law for mitochondrial metabolism*, we determined the specific expressions of work rates in the second law of thermodynamics (*Equation 32*), accounting for the free energy exchanges between mitochondria and their surroundings that balance dissipation and maintain the mitochondrial metabolism out of equilibrium. The thermodynamic efficiency of mitochondrial metabolism is defined by identifying which of these terms play the role of free energy input and output. To do so, we further split the nonconservative work rate (*Equation 47*) by recognizing that the effective reaction (*Equation 35*) is given by the sum of 2 (mass balanced) reactions



The effective reaction *Equation 55* corresponds to the net production (output) of free energy (ATP_c) by mitochondrial metabolism, while the effective reactions *Equation 56* and *Equation 36* represent a free energy input generated by the chemical potential gradient between oxygen, coenzymes, protons and carbon substrates. This allows us to write the nonconservative work rate (*Equation 47*) as

$$\dot{w}_{\text{nc}} = \Delta_r G'_{r_{\text{in}}^{\text{I}}} I^{\text{ATP}_c} + \Delta_r G'_{r_{\text{out}}^{\text{I}}} I^{\text{ATP}_c} + \Delta_r G'_{r_2} I^{\text{H}^+}. \quad (57)$$

The thermodynamic efficiency at steady state is thus given by

$$\eta = -\frac{\Delta_r G'_{r_{\text{out}}^{\text{I}}} I^{\text{ATP}_c}}{\Delta_r G'_{r_{\text{in}}^{\text{I}}} I^{\text{ATP}_c} + \Delta_r G'_{r_2} I^{\text{H}^+}}. \quad (58)$$

In the oscillatory regime we also have to account for the free energy provided by the driving work and, therefore, the thermodynamic efficiency averaged over a period is

$$\eta_{t_p} = -\frac{\int_0^{t_p} dt \Delta_r G'_{r_{\text{out}}^{\text{I}}} I^{\text{ATP}_c}}{\int_0^{t_p} dt \left(\Delta_r G'_{r_{\text{in}}^{\text{I}}} I^{\text{ATP}_c} + \Delta_r G'_{r_2} I^{\text{H}^+} + \dot{w}_{\text{driv}} \right)}. \quad (59)$$

In both cases, the thermodynamic efficiency quantify the amount of energy released by the synthesis of ATP normalized by the amount of energy injected in the mitochondria. In the main text, we use the notation $\bar{\eta}$ to refer to the average efficiency at steady-state or in the oscillatory regime.

Acknowledgments

WV is funded by the Complex Living Systems Initiative at the University of Luxembourg. FA and ME are funded by the Luxembourg National Research Fund, grant ChemComplex (C21/MS/16356329). GF is funded by the European Union – NextGenerationEU – and by the program STARS@UNIPD with project “ThermoComplex”. FA, AS and ME acknowledge financial support of the Institute for Advanced Studies of the University of Luxembourg through an Audacity Grant (IDAE-2020).

References

- Alberty RA. Thermodynamics of Biochemical Reactions. Hoboken, New Jersey: John Wiley & Sons; 2003.
- Avanzini F, Esposito M. Thermodynamics of concentration vs flux control in chemical reaction networks. J Chem Phys. 2022; 156(1):014116. doi: 10.1063/5.0076134.
- Avanzini F, Falasco G, Esposito M. Thermodynamics of non-elementary chemical reaction networks. New J Phys. 2020; 22(9):093040. doi: 10.1088/1367-2630/abafea.
- Avanzini F, Freitas N, Esposito M. Circuit Theory for Chemical Reaction Networks. Phys Rev X. 2023; 13(2):021041. doi: 10.1103/PhysRevX.13.021041.
- Avanzini F, Penocchio E, Falasco G, Esposito M. Nonequilibrium thermodynamics of non-ideal chemical reaction networks. J Chem Phys. 2021; 154(9):094114. doi: 10.1063/5.0041225.

Table 1. Chemical reactions incorporated into the kinetic model. Controlled species are in gray. Subscripts c, ER and m refer to the cytosol, the endoplasmic reticulum and the mitochondria, respectively.

Calcium exchanges and cytosolic ATP dynamics	
ERout	$\text{Ca}_{\text{ER}}^{2+} \xrightleftharpoons{\text{IP}_3} \text{Ca}_{\text{c}}^{2+}$
SERCA	$2 \text{Ca}_{\text{c}}^{2+} + \text{ATP}_{\text{c}} + \text{H}_2\text{O}_{\text{c}} \rightleftharpoons 2 \text{Ca}_{\text{ER}}^{2+} + \text{ADP}_{\text{c}} + \text{Pi}_{\text{c}}$
NCX	$\text{Ca}_{\text{m}}^{2+} + 3 \text{Na}_{\text{c}}^{+} \rightleftharpoons \text{Ca}_{\text{c}}^{2+} + 3 \text{Na}_{\text{m}}^{+}$
UNI	$\text{Ca}_{\text{c}}^{2+} \rightleftharpoons \text{Ca}_{\text{m}}^{2+}$
Hyd	$\text{ATP}_{\text{c}} + \text{H}_2\text{O}_{\text{c}} \rightleftharpoons \text{ADP}_{\text{c}} + \text{Pi}_{\text{c}}$
Electron transport chain and oxidative phosphorylation	
OX	$\text{NADH} + 10 \text{H}_{\text{m}}^{+} + \frac{1}{2} \text{O}_2 \rightleftharpoons \text{NAD} + 10 \text{H}_{\text{c}}^{+} + \text{H}_2\text{O}_{\text{m}}$
F1	$\text{ADP}_{\text{m}} + \text{Pi}_{\text{m}} + 3 \text{H}_{\text{c}}^{+} \rightleftharpoons \text{ATP}_{\text{m}} + \text{H}_2\text{O}_{\text{m}} + 3 \text{H}_{\text{m}}^{+}$
TCA cycle	
CS	$\text{OAA} + \text{AcCoA} + \text{H}_2\text{O}_{\text{m}} \rightleftharpoons \text{CIT} + \text{CoA}$
ACO	$\text{CIT} \rightleftharpoons \text{ISOC}$
IDH	$\text{ISOC} + \text{NAD} \rightleftharpoons \alpha\text{KG} + \text{NADH} + \text{CO}_2$
KGDH	$\alpha\text{KG} + \text{NAD} + \text{CoA} \rightleftharpoons \text{SCoA} + \text{NADH} + \text{CO}_2$
SL	$\text{SCoA} + \text{ADP}_{\text{m}} + \text{Pi}_{\text{m}} \rightleftharpoons \text{SUC} + \text{ATP}_{\text{m}} + \text{CoA}$
SDH	$\text{SUC} + \text{CoQ} \rightleftharpoons \text{FUM} + \text{CoQH}_2$
FH	$\text{FUM} + \text{H}_2\text{O}_{\text{m}} \rightleftharpoons \text{MAL}$
MDH	$\text{MAL} + \text{NAD} \rightleftharpoons \text{OAA} + \text{NADH}$
Other exchange processes	
ANT	$\text{ATP}_{\text{m}} + \text{ADP}_{\text{c}} \rightleftharpoons \text{ATP}_{\text{c}} + \text{ADP}_{\text{m}}$
HI	$\text{H}_{\text{c}}^{+} \rightleftharpoons \text{H}_{\text{m}}^{+}$

Table 2. Fluxes of the system. V_{ref} is the volume of reference with respect to which each reaction rate, J_k , and the corresponding entropy production rate, σ_k , are normalized. Starting from the corresponding pseudoisomer concentrations, Magnus and Keizer estimate that $[ATP^{4-}]_c = 0.05 [ATP]_c$, $[ATP^{4-}]_m = 0.05 [ATP]_m$, $[ADP^{3-}]_c = 0.45 [ADP]_c$ and $[ADP^{3-}]_m = 0.36 [ADP]_m$.

Process	V_{ref}	J_k (mM s ⁻¹)	Ref.
ACO	V_m	$J_{ACO} = k_f^{ACO} \left([CIT]_m - \frac{[ISOC]_m}{K_{ACO}} \right)$	<i>Cortassa et al. (2003)</i>
ANT	V_m	$J_{ANT} = V_{max}^{ANT} \frac{1 - \frac{[ATP^{4-}]_c [ADP^{3-}]_m e^{-\Delta\Psi}}{[ATP^{4-}]_m [ADP^{3-}]_c}}{\left(1 + \frac{[ATP^{4-}]_c e^{-\frac{fF\Delta\Psi}{RT}}}{[ADP^{3-}]_c} \right) \left(1 + \frac{[ADP^{3-}]_m}{[ATP^{4-}]_m} \right)}$	<i>Magnus and Keizer (1997)</i>
CS	V_m	$J_{CS} = \frac{V_{max}^{CS}}{1 + \frac{K_{M,AcCoA}}{[AcCoA]_m} + \frac{K_{M,OAA}}{[OAA]_m} \left(1 + \frac{[AcCoA]_m}{K_{i,AcCoA}} \right) + \frac{K_{S,AcCoA} K_{M,OAA}}{([OAA]_m [AcCoA]_m)}}$	<i>Dudycha (2000)</i>
ERout	V_c	$J_{ERout} = \left(V_{max}^{IP_3R} \frac{[IP_3]^2}{[IP_3]^2 + K_{a,IP_3}^2} \frac{[Ca^{2+}]_c}{[Ca^{2+}]_c + K_{a,Ca}^2} \frac{K_{i,Ca}^4}{K_{i,Ca}^4 + [Ca^{2+}]_c^4} + V^{LEAK} \right) ([Ca^{2+}]_{ER} - [Ca^{2+}]_c)$	<i>Komin et al. (2015)</i>
F1	V_m	$J_{F1} = -\rho_{f1} \frac{\left[\rho_a 10^{3\Delta pH} + \rho_{c1} e^{-\frac{3F\Delta\Psi}{RT}} \right] A_{F1} - \rho_a e^{-\frac{3F\Delta\Psi}{RT}} + \rho_{c2} A_{F1} e^{-\frac{3F\Delta\Psi}{RT}}}{[1 + \rho_1 A_{F1}] e^{-\frac{3F\Delta\Psi}{RT}} + [\rho_2 + \rho_3 A_{F1}] e^{-\frac{3F\Delta\Psi}{RT}}}$ with $A_{F1} = K_{F1} \frac{[ATP]_m}{[ADP]_m [Pi]_m}$	<i>Magnus and Keizer (1997)</i>
FH	V_m	$J_{FH} = k_f^{FH} \left([FUM]_m - \frac{[MAL]_m}{K_{FH}} \right)$	<i>Cortassa et al. (2003)</i>
HI	V_m	$J_{HI} = g_H \left(\Delta\Psi - 2.303 \frac{RT}{F} \Delta pH \right)$	<i>Magnus and Keizer (1997)</i>
Hyd	V_c	$J_{Hyd} = k_{Hyd} \frac{[ATP]_c}{[ATP]_c + K_{M,ATPc}}$	<i>Wacquier et al. (2016)</i>
IDH	V_m	$J_{IDH} = \frac{v^{IDH}_{max}}{1 + \frac{[H]_m}{k_{h,1}} + \frac{k_{h,2}}{[H]_m} + \frac{\left(\frac{K_{M,ISOC}}{[ISOC]_m} \right)^{n_I}}{\left(1 + \frac{[ADP]_m}{K_{a,ADP}} \right) \left(1 + \frac{[Ca^{2+}]_m}{K_{a,CaM}} \right)} + \frac{K_{M,NAD}}{[NAD]_m} \left(1 + \frac{[NADH]_m}{K_{i,NADH}} \right) + \frac{\left(\frac{K_{M,ISOC}}{[ISOC]_m} \right)^{n_I} \frac{K_{i,IDH}}{K_{M,NAD}} \left(1 + \frac{[NADH]_m}{K_{i,NADH}} \right)}{\left(1 + \frac{[ADP]_m}{K_{a,ADP}} \right) \left(1 + \frac{[Ca^{2+}]_m}{K_{a,CaM}} \right)}$	<i>Cortassa et al. (2003)</i>
KGDH	V_m	$J_{KGDH} = \frac{V_{max}^{KGDH}}{1 + \frac{K_{M,Mg}}{[Mg^{2+}]_m} + \frac{K_{M,NAD}}{[NAD]_m}} \frac{v_{\alpha KG}}{\left(1 + \frac{[Mg^{2+}]_m}{K_{D,Mg}} \right) \left(1 + \frac{[Ca^{2+}]_m}{K_{D,Ca}} \right)}$	<i>Dudycha (2000)</i>
MDH	V_m	$J_{MDH} = V_{max}^{MDH} \frac{[MAL]_m [NAD]_m - \frac{[OAA]_m [NADH]_m}{K_{MDH}}}{\left(1 + \frac{[MAL]_m}{K_{M,MAL}} \right) \left(1 + \frac{[NAD]_m}{K_{M,NAD}} \right) + \left(1 + \frac{[OAA]_m}{K_{M,OAA}} \right) \left(1 + \frac{[NADH]_m}{K_{M,NADH}} \right) - 1}$	<i>Berndt et al. (2015)</i>
NCX	V_m	$J_{NCX} = V_{max}^{NCX} \frac{e^{-\frac{bF(\Delta\Psi - \Delta\Psi^*)}{RT}}}{\left(1 + \frac{K_{M,Na}}{[Na^+]_c} \right)^n \left(1 + \frac{K_{M,Ca}}{[Ca^{2+}]_m} \right)}$	<i>Magnus and Keizer (1997)</i>
Ox	V_m	$J_{Ox} = \frac{1}{2} \rho_{res} \frac{\left[r_a 10^{6\Delta pH} + r_{c1} e^{-\frac{6F\Delta\Psi}{RT}} \right] A_{res} - r_a e^{-\frac{6F\Delta\Psi}{RT}} + r_{c2} A_{res} e^{-\frac{6F\Delta\Psi}{RT}}}{[1 + r_1 A_{res}] e^{-\frac{6F\Delta\Psi}{RT}} + [r_2 + r_3 A_{res}] e^{-\frac{6F\Delta\Psi}{RT}}}$ with $A_{res} = K_{res} \sqrt{\frac{[NADH]_m}{[NAD]_m}}$	<i>Magnus and Keizer (1997)</i>
SDH	V_m	$J_{SDH} = \frac{v^{SDH}_{max}}{1 + \frac{K_{M,SUC}}{[SUC]_m} \left(1 + \frac{[OAA]_m}{K_{i,OAA}} \right) \left(1 + \frac{[FUM]_m}{K_{i,FUM}} \right)}$	<i>Cortassa et al. (2003)</i>
SERCA	V_c	$J_{SERCA} = V_{max}^{SERCA} \frac{[Ca^{2+}]_c}{[Ca^{2+}]_c + K_{Ca}^2} \frac{[ATP]_c}{[ATP]_c + K_{ATPc}}$	<i>Wacquier et al. (2016)</i>
SL	V_m	$J_{SL} = k_f^{SL} \left([SCoA]_m [ADP]_m [Pi]_m - \frac{[SUC]_m [ATP]_m [CoA]_m}{K_{SL}} \right)$	<i>Wei et al. (2011)</i>
UNI	V_m	$J_{UNI} = V_{max}^{UNI} \frac{2F(\Delta\Psi - \Delta\Psi^*)}{RT \left(1 - e^{-\frac{2F(\Delta\Psi - \Delta\Psi^*)}{RT}} \right)} \frac{\left[\frac{[Ca^{2+}]_c}{K_{trans}} \left(1 + \frac{[Ca^{2+}]_c}{K_{trans}} \right) \right]^3}{\left(1 + \frac{[Ca^{2+}]_c}{K_{trans}} \right)^4 + \frac{l}{\left(1 + \frac{[Ca^{2+}]_c}{K_{act}} \right)^{n_a}}}$	<i>Magnus and Keizer (1997)</i>

Table 3. Forces of the system. Transformed Gibbs free energies of reaction ($\Delta_r G'_k$) associated to each process of the system. The indices c and m associated to $\Delta_r G'_k$ indicate that this thermodynamic quantity is evaluated at cytosolic and mitochondrial pH, that is, pH = 7.2 and pH = 8.0, respectively. The value of $\Delta_r G'_k$, which also accounts for physiological ionic strength ($I = 0.12$ M *Robinson et al. (2006)*) and $[\text{Mg}^{2+}]_m$ (pMg=3.4), was retrieved for each relevant process *via* Equilibrator *Flamholz et al. (2012)*. Starting from the corresponding pseudoisomer concentrations, Magnus and Keizer estimate that $[\text{ATP}^{4-}]_c = 0.05 [\text{ATP}]_c$, $[\text{ATP}^{4-}]_m = 0.05 [\text{ATP}]_m$, $[\text{ADP}^{3-}]_c = 0.45 [\text{ADP}]_c$ and $[\text{ADP}^{3-}]_m = 0.36 [\text{ADP}]_m$.

Process	$\Delta_r G'_k$ (J mol ⁻¹)	
ACO	$\Delta_r G'_{\text{ACO},m} = \Delta_r G'^{\circ}_{\text{ACO},m} + RT \ln \frac{[\text{ISOC}]_m}{[\text{CIT}]_m}$	$\Delta_r G'^{\circ}_{\text{ACO},m} = 6700 \text{ J mol}^{-1}$
ANT	$\Delta_r G'_{\text{ANT},m} = RT \ln \frac{[\text{ATP}^{4-}]_c [\text{ADP}^{3-}]_m}{[\text{ATP}^{4-}]_m [\text{ADP}^{3-}]_c} - F \Delta \Psi$	
CS	$\Delta_r G'_{\text{CS},m} = \Delta_r G'^{\circ}_{\text{CS},m} + RT \ln \frac{[\text{CIT}]_m [\text{CoA}]_m}{[\text{OAA}]_m [\text{AcCoA}]_m}$	$\Delta_r G'^{\circ}_{\text{CS},m} = -41200 \text{ J mol}^{-1}$
ERout	$\Delta_r G'_{\text{ERout},c} = RT \ln \frac{[\text{Ca}^{2+}]_c}{[\text{Ca}^{2+}]_{\text{ER}}}$	
F1	$\Delta_r G'_{\text{F1},m} = -\Delta_r G'_{\text{Hyd},m} + RT \ln \frac{[\text{H}]_m^3 [\text{ATP}]_m}{[\text{H}]_c^3 [\text{ADP}]_m [\text{Pi}]_m} - 3F \Delta \Psi$	$\Delta_r G'_{\text{Hyd},m} = -32200 \text{ J mol}^{-1}$
FH	$\Delta_r G'_{\text{FH},m} = \Delta_r G'^{\circ}_{\text{FH},m} + RT \ln \frac{[\text{MAL}]_m}{[\text{FUM}]_m}$	$\Delta_r G'^{\circ}_{\text{FH},m} = -3400 \text{ J mol}^{-1}$
HI	$\Delta_r G'_{\text{HI},m} = RT \ln \frac{[\text{H}]_m}{[\text{H}]_c} - F \Delta \Psi$	
Hyd	$\Delta_r G'_{\text{Hyd},c} = \Delta_r G'^{\circ}_{\text{Hyd},c} + RT \ln \frac{[\text{ADP}]_c [\text{Pi}]_c}{[\text{ATP}]_c}$	$\Delta_r G'^{\circ}_{\text{Hyd},c} = -28300 \text{ J mol}^{-1}$
IDH	$\Delta_r G'_{\text{IDH},m} = \Delta_r G'^{\circ}_{\text{IDH},m} + RT \ln \frac{[\alpha\text{KG}]_m [\text{CO}_2]_m [\text{NADH}]_m}{[\text{ISOC}]_m [\text{NAD}]_m}$	$\Delta_r G'^{\circ}_{\text{IDH},m} = 5100 \text{ J mol}^{-1}$
KGDH	$\Delta_r G'_{\text{KGDH},m} = \Delta_r G'^{\circ}_{\text{KGDH},m} + RT \ln \frac{[\text{SCoA}]_m [\text{NADH}]_m [\text{CO}_2]_m}{[\alpha\text{KG}]_m [\text{NAD}]_m [\text{CoA}]_m}$	$\Delta_r G'^{\circ}_{\text{KGDH},m} = -27600 \text{ J mol}^{-1}$
MDH	$\Delta_r G'_{\text{MDH},m} = \Delta_r G'^{\circ}_{\text{MDH},m} + RT \ln \frac{[\text{OAA}]_m [\text{NADH}]_m}{[\text{NAD}]_m [\text{MAL}]_m}$	$\Delta_r G'^{\circ}_{\text{MDH},m} = 24200 \text{ J mol}^{-1}$
NCX	$\Delta_r G'_{\text{NCX},m} = RT \ln \frac{[\text{Ca}^{2+}]_c [\text{Na}]_m^3}{[\text{Ca}^{2+}]_m [\text{Na}]_c^3} - F \Delta \Psi$	
Ox	$\Delta_r G'_{\text{Ox},m} = \Delta_r G'^{\circ}_{\text{Ox},m} + RT \ln \frac{[\text{H}]_c^{10} [\text{NAD}]_m}{[\text{H}]_m^{10} [\text{NADH}]_m [\text{O}_2]_m^{0.5}} + 10F \Delta \Psi$	$\Delta_r G'^{\circ}_{\text{Ox},m} = -225300 \text{ J mol}^{-1}$
SDH	$\Delta_r G'_{\text{SDH},m} = \Delta_r G'^{\circ}_{\text{SDH},m} + RT \ln \frac{[\text{FUM}]_m [\text{CoQH}_2]_m}{[\text{SUC}]_m [\text{CoQ}]_m}$	$\Delta_r G'^{\circ}_{\text{SDH},m} = -24200 \text{ J mol}^{-1}$
SERCA	$\Delta_r G'_{\text{SERCA},c} = \Delta_r G'_{\text{Hyd},c} + RT \ln \frac{[\text{ADP}]_c [\text{Pi}]_c [\text{Ca}^{2+}]_{\text{ER}}^2}{[\text{ATP}]_c [\text{Ca}^{2+}]_c^2}$	$\Delta_r G'_{\text{Hyd},c} = -28300 \text{ J mol}^{-1}$
SL	$\Delta_r G'_{\text{SL},m} = \Delta_r G'^{\circ}_{\text{SL},m} + RT \ln \frac{[\text{SUC}]_m [\text{CoA}]_m [\text{ATP}]_m}{[\text{SCoA}]_m [\text{ADP}]_m [\text{Pi}]_m}$	$\Delta_r G'^{\circ}_{\text{SL},m} = 800 \text{ J mol}^{-1}$
UNI	$\Delta_r G'_{\text{UNI},m} = RT \ln \frac{[\text{Ca}^{2+}]_m}{[\text{Ca}^{2+}]_c} - 2F \Delta \Psi$	

Table 4. Reference parameter values.

Parameter	Definition	Value (units)	Ref.
α	Ratio between ER and cytosol volumes	0.10	<i>Wacquier et al. (2016)</i>
A_{tot}	Total concentration of cytosolic adenine nucleotides	3 mM	<i>Moein (2017)</i>
$A_{\text{m,tot}}$	Total concentration of mitochondrial adenine nucleotides	15 mM	<i>Magnus and Keizer (1997)</i>
b	Dependence of electrogenic $\text{Na}^+/\text{Ca}^{2+}$ exchanger on $\Delta\Psi$	0.5	<i>Magnus and Keizer (1997)</i>
C_m	Mitochondrial membrane capacitance	$1.812 \times 10^{-3} \text{ mM mV}^{-1}$	<i>Cortassa et al. (2003)</i>
$[\text{CO}_2]$	Total CO_2 concentration in mitochondrial matrix	21.4 mM	<i>Wu et al. (2007)</i>
$[\text{CoA}]$	CoA concentration in mitochondrial matrix	0.02 mM	<i>Cortassa et al. (2003)</i>
$[\text{CoQ}]$	CoQ concentration in mitochondrial matrix	0.97 mM	<i>Wu et al. (2007)</i>
$[\text{CoQH}_2]$	CoQ ₂ concentration in mitochondrial matrix	0.38 mM	<i>Wu et al. (2007)</i>
c_{tot}	Total free Ca^{2+} concentration of the cell normalized by V_c	1500 μM	This work
c_{Ktot}	Total concentration of TCA cycle intermediates	1 mM	<i>Cortassa et al. (2003)</i>
δ	Ratio between mitochondrial matrix and cytosol volumes	0.15	<i>Siess et al. (1976); Lund and Wiggins (1987)</i>
ΔpH	pH difference between cytosol and mitochondrial matrix ($\text{pH}_c - \text{pH}_m$)	-0.80	<i>Buckler and Vaughan-Jones (1990); Casey et al. (2010)</i>
$\Delta\Psi^*$	Membrane potential offset for Ca^{2+} transport	91 mV	<i>Magnus and Keizer (1997)</i>
$\Delta\Psi_B$	Total phase boundary potential	50 mV	<i>Magnus and Keizer (1997)</i>
F	Faraday constant	96.485 kC mol ⁻¹	
f	Fraction of $\Delta\Psi$ responsible for the behavior of ANT in energized mitochondria	0.5	<i>Magnus and Keizer (1997)</i>
f_c	Fraction of free cytosolic Ca^{2+}	0.01	<i>Wacquier et al. (2016)</i>
f_e	Fraction of free Ca^{2+} in the ER	0.01	<i>Wacquier et al. (2016)</i>
f_m	Fraction of free mitochondrial Ca^{2+}	0.0003	<i>Magnus and Keizer (1997)</i>
γ	Conversion factor between mM and μM	1000 $\mu\text{M mM}^{-1}$	
g	Fitting factor for voltage in respiration rate	0.85	<i>Magnus and Keizer (1997)</i>
g_{H}	Ionic conductance of the mitochondrial inner membrane	$10^{-5} \text{ mM mV}^{-1} \text{ s}^{-1}$	<i>Cortassa et al. (2003)</i>
$[\text{H}^+]_c$	Cytosolic proton concentration	$6.31 \times 10^{-5} \text{ mM}$	<i>Buckler and Vaughan-Jones (1990); Casey et al. (2010)</i>
$[\text{H}^+]_m$	Concentration of proton in the mitochondrial matrix	10^{-5} mM	<i>Buckler and Vaughan-Jones (1990); Casey et al. (2010)</i>
$K_{\text{a,Cac}}$	Activation constant of IP_3Rs for cytosolic Ca^{2+}	0.60 μM	This work
K_{ACO}	Equilibrium constant of ACO	0.067	<i>Flamholz et al. (2012); Berndt et al. (2015)</i>
K_{act}	Dissociation constant of mitochondrial uniporter for activating Ca^{2+}	0.38	<i>Magnus and Keizer (1997)</i>
K_{ATPc}	Dissociation constant of SERCA for cytosolic ATP	0.05 mM	<i>Scofano et al. (1979); Moein (2017)</i>
$K_{\text{a,ADP}}$	Activation constant of IDH for ADP_m	0.062 mM	<i>Dudycha (2000); Cortassa et al. (2003)</i>
$K_{\text{a,Cam}}$	Activation constant of IDH for mitochondrial Ca^{2+}	1.41 μM	<i>Cortassa et al. (2003)</i>
$K_{\text{a,IP}_3}$	Activation constant of IP_3Rs for IP_3	1.00 μM	<i>Dupont and Erneux (1997); Wacquier et al. (2016)</i>
K_{Ca}	Dissociation constant of SERCA for Ca^{2+}	0.35 μM	<i>Dupont and Erneux (1997); Wacquier et al. (2016)</i>
$K_{\text{D,Ca}}$	Dissociation constant of KGDH for mitochondrial Ca^{2+}	1.27 μM	<i>Dudycha (2000); Cortassa et al. (2003)</i>
$K_{\text{D,Mg}}$	Dissociation constant of KGDH for mitochondrial Mg^{2+}	0.0308 mM	<i>Cortassa et al. (2003)</i>
K_{FI}	Equilibrium constant for ATP hydrolysis in mitochondrial matrix	1.71×10^6	<i>Pietrobon and Caplan (1985); Cortassa et al. (2003)</i>
K_{FH}	Equilibrium constant for FH	3.942	<i>Flamholz et al. (2012)</i>
$k_{\text{f}}^{\text{ACO}}$	Forward rate constant of ACO	12.5 s ⁻¹	<i>Cortassa et al. (2003)</i>
k_{f}^{FH}	Forward rate constant of FH	8.3 s ⁻¹	This work
k_{f}^{SL}	Forward rate constant of SL	$0.127 \text{ mM}^{-2} \text{ s}^{-1}$	<i>Cortassa et al. (2003)</i>
$k_{\text{h},1}$	First ionization constant of IDH	$8.1 \times 10^{-5} \text{ mM}$	<i>Dudycha (2000); Cortassa et al. (2003)</i>
$k_{\text{h},2}$	Second ionization constant of IDH	$5.98 \times 10^{-5} \text{ mM}$	<i>Dudycha (2000); Cortassa et al. (2003)</i>
k_{Hyd}	Hydrolysis rate of ATP_c due to cellular activity	$2 \times 10^{-2} \text{ mM s}^{-1}$	This work
$K_{\text{i,AcCoA}}$	Inhibition constant of CS for AcCoA	$3.7068 \times 10^{-2} \text{ mM}$	<i>Dudycha (2000)</i>
$K_{\text{i,Ca}}$	Inhibition constant of IP_3Rs for cytosolic Ca^{2+}	1.00 μM	This work
$K_{\text{i,FUM}}$	Inhibition constant of SDH for fumarate	1.3 mM	<i>Cortassa et al. (2003)</i>
$K_{\text{i,OGA}}$	Inhibition constant of SDH for oxaloacetate	0.15 mM	<i>Cortassa et al. (2003)</i>
$K_{\text{i,NADH}}$	Inhibition constant of IDH for NADH	0.19 mM	<i>Cortassa et al. (2003)</i>
$K_{\text{M,AcCoA}}$	Michaelis constant of CS for acetyl-CoA	$1.2614 \times 10^{-2} \text{ mM}$	<i>Dudycha (2000); Cortassa et al. (2003)</i>
$K_{\text{M,KG}}$	Michaelis constant of KGDH for α -ketoglutarate	1.94 mM	<i>Cortassa et al. (2003)</i>
$K_{\text{M,ATPc}}$	Michaelis constant for ATP_c hydrolysis due to cellular activity	1 mM	<i>Wacquier et al. (2016)</i>
$K_{\text{M,Ca}}$	Michaelis constant of $\text{Na}^+/\text{Ca}^{2+}$ exchanger for Ca^{2+}	0.375 μM	<i>Cortassa et al. (2003)</i>
$K_{\text{M,ISOC}}$	Michaelis constant of IDH for isocitrate	1.52 mM	<i>Dudycha (2000); Cortassa et al. (2003)</i>
$K_{\text{M,MAL}}$	Michaelis constant of MDH for malate	0.145 mM	<i>Berndt et al. (2015)</i>
$K_{\text{M,Na}}$	Michaelis constant of $\text{Na}^+/\text{Ca}^{2+}$ exchanger for Na^+	9.4 mM	<i>Magnus and Keizer (1997)</i>
$K_{\text{M,NAD}}^{\text{IDH}}$	Michaelis constant of IDH for NAD	0.923 mM	<i>Dudycha (2000); Cortassa et al. (2003)</i>
$K_{\text{M,NAD}}^{\text{KGDH}}$	Michaelis constant of KGDH for NAD	$3.87 \times 10^{-2} \text{ mM}$	This work
$K_{\text{M,NAD}}^{\text{MDH}}$	Michaelis constant of MDH for NAD	0.06 mM	<i>Berndt et al. (2015)</i>
$K_{\text{M,NADH}}$	Michaelis constant of MDH for NADH	0.044 mM	<i>Cortassa et al. (2003)</i>

Table 4. Reference parameter values (continued).

Parameter	Definition	Value (units)	Ref.
$K_{M,LOAA}^{CS}$	Michaelis constant of CS for oxaloacetate	5×10^{-3} mM	<i>Matsuoka and Srere (1973); Kurz et al. (1995); Berndt et al. (2015)</i>
$K_{M,LOAA}^{MDH}$	Michaelis constant of MDH for oxaloacetate	0.017 mM	<i>Berndt et al. (2015)</i>
$K_{M,SUC}$	Michaelis constant of SDH for succinate	3×10^{-2} mM	<i>Cortassa et al. (2003)</i>
K_{MDH}	Equilibrium constant of MDH	2.756×10^{-5}	<i>Flamholz et al. (2012)</i>
K_{res}	Equilibrium constant of O ₂ reduction by NADH in mitochondrial matrix	1.35×10^{18}	<i>Magnus and Keizer (1997)</i>
$K_{s,AcCoA}$	Other binding constant of citrate synthase for AcCoA	8.0749×10^{-2} mM	<i>Dudycha (2000)</i>
K_{SL}	Equilibrium constant for SL	0.724	<i>Flamholz et al. (2012)</i>
K_{trans}	Dissociation constant of mitochondrial uniporter for translocated Ca ²⁺	19 μM	<i>Magnus and Keizer (1998a)</i>
L	Equilibrium constant for mitochondrial uniporter conformations	110	<i>Magnus and Keizer (1998a)</i>
$[Mg^{2+}]_m$	Mg concentration in the mitochondrial matrix	0.4 mM	<i>Cortassa et al. (2003)</i>
n	Number of Na ⁺ binding to electrogenic Na ⁺ /Ca ²⁺ exchanger	3	<i>Magnus and Keizer (1997)</i>
n_u	Mitochondrial uniporter activation cooperativity	2.8	<i>Magnus and Keizer (1997)</i>
$[Na^+]_c$	Cytosolic Na ⁺ concentration	10 mM	<i>Cortassa et al. (2003)</i>
$[Na^+]_m$	Mitochondrial Na ⁺ concentration	5 mM	<i>Donoso et al. (1992)</i>
$n_{\alpha KG}$	Hill coefficient of KGDH for αKG	1.2	<i>Cortassa et al. (2003)</i>
n_i	Hill coefficient of IDH for isocitrate	2	<i>Wei et al. (2011)</i>
N_{tot}	Total concentration of mitochondrial pyridine nucleotides	0.8 mM	This work
$[O_2]$	O ₂ concentration in mitochondrial matrix	2.6×10^{-5} M	<i>Beard (2005)</i>
p_1	Combination of elementary kinetic constants for the 6-state ATPase model	1.346×10^{-8}	<i>Magnus and Keizer (1997)</i>
p_2	Combination of elementary kinetic constants for the 6-state ATPase model	7.739×10^{-7}	<i>Magnus and Keizer (1997)</i>
p_3	Combination of elementary kinetic constants for the 6-state ATPase model	6.65×10^{-15}	<i>Magnus and Keizer (1997)</i>
p_a	Combination of elementary kinetic constants for the 6-state ATPase model	$1.656 \times 10^{-5} s^{-1}$	<i>Magnus and Keizer (1997)</i>
p_{c1}	Combination of elementary kinetic constants for the 6-state ATPase model	$9.651 \times 10^{-14} s^{-1}$	<i>Magnus and Keizer (1997)</i>
p_{c2}	Combination of elementary kinetic constants for the 6-state ATPase model	$4.845 \times 10^{-19} s^{-1}$	<i>Magnus and Keizer (1997)</i>
$[P_i]_c$	Inorganic phosphate concentration in cytosol	1 mM	<i>Bevington et al. (1986)</i>
$[P_i]_m$	Inorganic phosphate concentration in mitochondrial matrix	20 mM	<i>Magnus and Keizer (1997)</i>
R	Gas constant	$8.314 J mol^{-1} K^{-1}$	
ρ_{t1}	Density of ATPase pumps	1.5	This work
ρ_{res}	Density of H ⁺ pumps in mitochondrial membrane	1.00	This work
r_1	Combination of elementary kinetic constants for the 6-state respiration model	2.077×10^{-18}	<i>Magnus and Keizer (1997)</i>
r_2	Combination of elementary kinetic constants for the 6-state respiration model	1.728×10^{-9}	<i>Magnus and Keizer (1997)</i>
r_3	Combination of elementary kinetic constants for the 6-state respiration model	1.059×10^{-26}	<i>Magnus and Keizer (1997)</i>
r_a	Combination of elementary kinetic constants for the 6-state respiration model	$6.394 \times 10^{-10} s^{-1}$	<i>Magnus and Keizer (1997)</i>
r_{c1}	Combination of elementary kinetic constants for the 6-state respiration model	$2.656 \times 10^{-19} s^{-1}$	<i>Magnus and Keizer (1997)</i>
r_{c2}	Combination of elementary kinetic constants for the 6-state respiration model	$8.632 \times 10^{-27} s^{-1}$	<i>Magnus and Keizer (1997)</i>
T	Temperature	310 K	<i>Cortassa et al. (2003)</i>
V_{max}^{ANT}	Limiting rate of adenine nucleotide translocator (ANT)	15 mM s ⁻¹	<i>Cortassa et al. (2003)</i>
V_{max}^{CS}	Limiting rate of CS	52 mM s ⁻¹	This work
V_{max}^{IDH}	Limiting rate of IDH	0.15 mM s ⁻¹	This work
$V_{max}^{IP_3R}$	Limiting release rate of Ca ²⁺ through IP ₃ R	15 s ⁻¹	This work
V_{max}^{KGDH}	Limiting rate of KGDH	5 mM s ⁻¹	This work
V_{LEAK}	Leak rate of Ca ²⁺ from ER	0.15 s ⁻¹	This work
V_{max}^{MDH}	Limiting rate of MDH	32 mM s ⁻¹	This work
V_{max}^{NCX}	Limiting rate of Na ⁺ /Ca ²⁺ exchanger	2×10^{-3} mM s ⁻¹	This work
V_{max}^{SDH}	Limiting rate of SDH	1 mM s ⁻¹	This work
V_{max}^{SERCA}	Limiting rate of SERCA pumps	0.12 mM s ⁻¹	<i>Wacquier et al. (2016)</i>
V_{max}^{UNI}	Limiting rate of mitochondrial uniporter	0.30 mM s ⁻¹	This work

- Baiesi M**, Maes C. Life efficiency does not always increase with the dissipation rate. *J Phys Commun*. 2018; 2(4):045017. doi: 10.1088/2399-6528/aab654.
- Beard DA**. A Biophysical Model of the Mitochondrial Respiratory System and Oxidative Phosphorylation. *PLOS Comput Biol*. 2005; 1(4):e36. doi: 10.1371/journal.pcbi.0010036.
- Beard DA**, Liang Sd, Qian H. Energy Balance for Analysis of Complex Metabolic Networks. *Biophys J*. 2002; 83(1):79–86. doi: 10.1016/S0006-3495(02)75150-3.
- Berman MC**. Slippage and uncoupling in P-type cation pumps; implications for energy transduction mechanisms and regulation of metabolism. *BBA*. 2001; 1513(2):95–121. doi: 10.1016/S0005-2736(01)00356-X.
- Berndt N**, Kann O, Holzhütter HG. Physiology-based kinetic modeling of neuronal energy metabolism unravels the molecular basis of NAD(P)H fluorescence transients. *J Cereb Blood Flow Metab*. 2015; 35(9):1494–1506. doi: 10.1038/jcbfm.2015.70.
- Berridge MJ**, Bootman MD, Lipp P. Calcium—a life and death signal. *Nature*. 1998; 395(6703):645–648. doi: 10.1038/27094.
- Bertram R**, Gram Pedersen M, Luciani DS, Sherman A. A simplified model for mitochondrial ATP production. *J Theor Biol*. 2006; 243(4):575–586. doi: 10.1016/j.jtbi.2006.07.019.
- Bevington A**, Mundy KI, Yates AJP, Kanis JA, Russell RGG, Taylor DJ, Rajagopalan B, Radda GK. A study of intracellular orthophosphate concentration in human muscle and erythrocytes by ³¹P nuclear magnetic resonance spectroscopy and selective chemical assay. *Clin Sci*. 1986; 71(6):729–735. doi: 10.1042/cs0710729.
- Buckler KJ**, Vaughan-Jones RD. Application of a new pH-sensitive fluoroprobe (carboxy-SNARF-1) for intracellular pH measurement in small, isolated cells. *Pflugers Arch*. 1990; 417(2):234–239. doi: 10.1007/BF00370705.
- Calisto F**, Sousa FM, Sena FV, Refojo PN, Pereira MM. Mechanisms of Energy Transduction by Charge Translocating Membrane Proteins. *Chemical Reviews*. 2021; 121:1804–1844. doi: 10.1021/acs.chemrev.0c00830, publisher: American Chemical Society.
- Cao Y**, Wang H, Ouyang Q, Tu Y. The free-energy cost of accurate biochemical oscillations. *Nature Physics*. 2015 Sep; 11(9):772–778. doi: 10.1038/nphys3412.
- Casey JR**, Grinstein S, Orłowski J. Sensors and regulators of intracellular pH. *Nat Rev Mol Cell Biol*. 2010; 11(1):50–61. doi: 10.1038/nrm2820.
- Celsi F**, Pizzo P, Brini M, Leo S, Fotino C, Pinton P, Rizzuto R. Mitochondria, calcium and cell death: A deadly triad in neurodegeneration. *Biochim Biophys Acta*. 2009; 1787(5):335–344. doi: 10.1016/j.bbabi.2009.02.021.
- Cortassa S**, Aon MA, Marbán E, Winslow RL, O'Rourke B. An integrated model of cardiac mitochondrial energy metabolism and calcium dynamics. *Biophys J*. 2003; 84(4):2734–2755. doi: 10.1016/S0006-3495(03)75079-6.
- De Groot SR**, Mazur P. *Non-Equilibrium Thermodynamics*. New York: Dover; 1984.
- Dejos C**, Gkika D, Cantelmo AR. The Two-Way Relationship Between Calcium and Metabolism in Cancer. *Front Cell Dev Biol*. 2020; 8:573747.
- Denton RM**. Regulation of mitochondrial dehydrogenases by calcium ions. *BBA*. 2009; 1787(11):1309–1316. doi: 10.1016/j.bbabi.2009.01.005.
- Donoso P**, Mill JG, O'Neill SC, Eisner DA. Fluorescence measurements of cytoplasmic and mitochondrial sodium concentration in rat ventricular myocytes. *J Physiol*. 1992; 448(1):493–509. doi: 10.1113/jphysiol.1992.sp019053.
- Dudycha S**. A detailed model of the tricarboxylic acid cycle in heart cells. M.S. Dissertation, Johns Hopkins University; 2000.
- Dupont G**, Combettes L, Leybaert L. Calcium dynamics: spatio-temporal organization from the subcellular to the organ level. *Int Rev Cytol*. 2007; 261:193–245. doi: 10.1016/S0074-7696(07)61005-5.
- Dupont G**, Erneux C. Simulations of the effects of inositol 1,4,5-trisphosphate 3-kinase and 5-phosphatase activities on Ca²⁺ oscillations. *Cell Calcium*. 1997; 22(5):321–331. doi: 10.1016/S0143-4160(97)90017-8.
- Eisner DA**, Valdeolmillos M. A study of intracellular calcium oscillations in sheep cardiac Purkinje fibres measured at the single cell level. *J Physiol*. 1986; 372(1):539–556. doi: 10.1113/jphysiol.1986.sp016024.

- Estrada J**, Wong F, DePace A, Gunawardena J. Information Integration and Energy Expenditure in Gene Regulation. *Cell*. 2016; 166(1):234–244. doi: [10.1016/j.cell.2016.06.012](https://doi.org/10.1016/j.cell.2016.06.012).
- Falcke M**. Reading the patterns in living cells —the physics of Ca^{2+} signaling. *Adv Phys*. 2004; 53(3):255–440. doi: [10.1080/00018730410001703159](https://doi.org/10.1080/00018730410001703159).
- Filadi R**, Pizzo P. Mitochondrial calcium handling and neurodegeneration: when a good signal goes wrong. *Curr Opin Physiol*. 2020; 17:224–233. doi: [10.1016/j.cophys.2020.08.009](https://doi.org/10.1016/j.cophys.2020.08.009).
- Flamholz A**, Noor E, Bar-Even A, Liebermeister W, Milo R. Glycolytic strategy as a tradeoff between energy yield and protein cost. *Proc Natl Acad Sci USA*. 2013; 110(24):10039–10044. doi: [10.1073/pnas.1215283110](https://doi.org/10.1073/pnas.1215283110).
- Flamholz A**, Noor E, Bar-Even A, Milo R. eQuilibrator—the biochemical thermodynamics calculator. *Nucleic Acids Res*. 2012; 40(Database issue):D770–D775. doi: [10.1093/nar/gkr874](https://doi.org/10.1093/nar/gkr874).
- Giorgi C**, Agnoletto C, Bononi A, Bonora M, De Marchi E, Marchi S, Missiroli S, Patergnani S, Poletti F, Rimessi A, Suski JM, Wieckowski MR, Pinton P. Mitochondrial calcium homeostasis as potential target for mitochondrial medicine. *Mitochondrion*. 2012; 12(1):77–85. doi: [10.1016/j.mito.2011.07.004](https://doi.org/10.1016/j.mito.2011.07.004).
- Goldberg RN**, Tewari YB, Bhat TN. Thermodynamics of enzyme-catalyzed reactions—a database for quantitative biochemistry. *Bioinformatics*. 2004; 20(16):2874–2877. doi: [10.1093/bioinformatics/bth314](https://doi.org/10.1093/bioinformatics/bth314).
- Goloubinoff P**, Sassi AS, Fauvet B, Barducci A, De Los Rios P. Chaperones convert the energy from ATP into the nonequilibrium stabilization of native proteins. *Nat Chem Biol*. 2018; 14(4):388–395. doi: [10.1038/s41589-018-0013-8](https://doi.org/10.1038/s41589-018-0013-8).
- Griffiths EJ**, Rutter GA. Mitochondrial calcium as a key regulator of mitochondrial ATP production in mammalian cells. *Biochimica et Biophysica Acta (BBA) - Bioenergetics*. 2009; 1787(11):1324–1333. doi: [10.1016/j.bbabi.2009.01.019](https://doi.org/10.1016/j.bbabi.2009.01.019).
- Gräber P**, Milazzo G. *Bioenergetics. Bioelectrochemistry: Principles and Practice*, Basel: Birkhäuser; 1997. doi: [10.1007/978-3-0348-8994-0](https://doi.org/10.1007/978-3-0348-8994-0).
- Guerrero-Hernandez A**, Verkhratsky A. Calcium signalling in diabetes. *Cell Calcium*. 2014; 56(5):297–301. doi: [10.1016/j.ceca.2014.08.009](https://doi.org/10.1016/j.ceca.2014.08.009).
- Hajnoczky G**, Robb-Gaspers LD, Seitz MB, Thomas AP. Decoding of cytosolic calcium oscillations in the mitochondria. *Cell*. 1995; 82(3):415–424. doi: [10.1016/0092-8674\(95\)90430-1](https://doi.org/10.1016/0092-8674(95)90430-1).
- Hill TL**. *Free Energy Transduction in Biology: The Steady-State Kinetic and Thermodynamic Formalism*. New York: Academic Press; 2012.
- Jouaville LS**, Ichas F, Holmuhamedov EL, Camacho P, Lechleiter JD. Synchronization of calcium waves by mitochondrial substrates in *Xenopus laevis* oocytes. *Nature*. 1995; 377(6548):438–441. doi: [10.1038/377438a0](https://doi.org/10.1038/377438a0).
- Komin N**, Moein M, Ellisman MH, Skupin A. Multiscale Modeling Indicates That Temperature Dependent $[Ca^{2+}]_i$ Spiking in Astrocytes Is Quantitatively Consistent with Modulated SERCA Activity. *Neural Plast*. 2015; 2015:683490. doi: [10.1155/2015/683490](https://doi.org/10.1155/2015/683490).
- Kurz LC**, Shah S, Frieden C, Nakra T, Stein RE, Drysdale GR, Evans CT, Srere PA. Catalytic strategy of citrate synthase: subunit interactions revealed as a consequence of a single amino acid change in the oxaloacetate binding site. *Biochemistry*. 1995; 34(41):13278–13288. doi: [10.1021/bi00041a003](https://doi.org/10.1021/bi00041a003).
- Lund P**, Wiggins D. The matrix water space of mitochondria in situ in isolated hepatocytes. *Biosci Rep*. 1987; 7(1):59–66. doi: [10.1007/BF01122728](https://doi.org/10.1007/BF01122728).
- Magnus G**, Keizer J. Minimal model of beta-cell mitochondrial Ca^{2+} handling. *A J Physiol*. 1997; 273(2 Pt 1):C717–733. doi: [10.1152/ajpcell.1997.273.2.C717](https://doi.org/10.1152/ajpcell.1997.273.2.C717).
- Magnus G**, Keizer J. Model of beta-cell mitochondrial calcium handling and electrical activity. I. Cytoplasmic variables. *Am J Physiol*. 1998; 274(4):C1158–1173. doi: [10.1152/ajpcell.1998.274.4.C1158](https://doi.org/10.1152/ajpcell.1998.274.4.C1158).
- Magnus G**, Keizer J. Model of beta-cell mitochondrial calcium handling and electrical activity. II. Mitochondrial variables. *Am J Physiol*. 1998; 274(4):C1174–1184. doi: [10.1152/ajpcell.1998.274.4.C1174](https://doi.org/10.1152/ajpcell.1998.274.4.C1174).
- Matsuoka Y**, Srere PA. Kinetic Studies of Citrate Synthase from Rat Kidney and Rat Brain. *J Biol Chem*. 1973; 248(23):8022–8030. doi: [10.1016/S0021-9258\(19\)43188-8](https://doi.org/10.1016/S0021-9258(19)43188-8).

- McCormack JG.** Characterization of the effects of Ca²⁺ on the intramitochondrial Ca²⁺-sensitive enzymes from rat liver and within intact rat liver mitochondria. *Biochem J.* 1985; 231(3):581–595. doi: 10.1042/bj2310581.
- Moein M.** Dissecting the crosstalk between intracellular calcium signalling and mitochondrial metabolism. PhD Thesis, University of Luxembourg; 2017.
- Monteith GR,** Prevarskaya N, Roberts-Thomson SJ. The calcium–cancer signalling nexus. *Nat Rev Cancer.* 2017; 17(6):373–380. doi: 10.1038/nrc.2017.18.
- Nicholls DG,** Ferguson SJ. *Bioenergetics 2.* San Diego: Academic Press; 1992.
- Niebel B,** Leupold S, Heinemann M. An upper limit on Gibbs energy dissipation governs cellular metabolism. *Nat Metab.* 2019; 1(1):125–132. doi: 10.1038/s42255-018-0006-7.
- Noor E,** Bar-Even A, Flamholz A, Lubling Y, Davidi D, Milo R. An integrated open framework for thermodynamics of reactions that combines accuracy and coverage. *Bioinformatics.* 2012; 28(15):2037–2044. doi: 10.1093/bioinformatics/bts317.
- Noor E,** Flamholz A, Liebermeister W, Bar-Even A, Milo R. A note on the kinetics of enzyme action: A decomposition that highlights thermodynamic effects. *FEBS Lett.* 2013 Sep; 587(17):2772–2777. doi: 10.1016/j.febslet.2013.07.028.
- Noor E,** Haraldsdóttir HS, Milo R, Fleming RMT. Consistent Estimation of Gibbs Energy Using Component Contributions. *PLoS Comput Biol.* 2013; 9(7):e1003098. doi: 10.1371/journal.pcbi.1003098.
- Parrondo JMR,** Horowitz JM, Sagawa T. Thermodynamics of information. *Nature Phys.* 2015; 11(2):131–139. doi: 10.1038/nphys3230.
- Pietrobon D,** Caplan SR. Flow-force relationships for a six-state proton pump model: intrinsic uncoupling, kinetic equivalence of input and output forces, and domain of approximate linearity. *Biochemistry.* 1985; 24(21):5764–5776. doi: 10.1021/bi00342a012.
- Rao R,** Esposito M. Nonequilibrium Thermodynamics of Chemical Reaction Networks: Wisdom from Stochastic Thermodynamics. *Phys Rev X.* 2016; 6(4):041064. doi: 10.1103/PhysRevX.6.041064.
- Rao R,** Esposito M. Conservation laws and work fluctuation relations in chemical reaction networks. *J Chem Phys.* 2018; 149(24):245101. doi: 10.1063/1.5042253.
- Robinson PJJ,** Fairall L, Huynh VAT, Rhodes D. EM measurements define the dimensions of the “30-nm” chromatin fiber: Evidence for a compact, interdigitated structure. *Proc Natl Acad Sci USA.* 2006; 103(17):6506–6511. doi: 10.1073/pnas.0601212103.
- Rodenfels J,** Neugebauer KM, Howard J. Heat Oscillations Driven by the Embryonic Cell Cycle Reveal the Energetic Costs of Signaling. *Dev Cell.* 2019; 48(5):646–658.e6. doi: 10.1016/j.devcel.2018.12.024.
- Rubi JM,** Naspreda M, Kjelstrup S, Bedeaux D. Energy Transduction in Biological Systems: A Mesoscopic Non-Equilibrium Thermodynamics Perspective. *J Non-Equilib Thermodyn.* 2007; 32(4):351–378. doi: 10.1515/JNETDY.2007.027.
- Sartori P,** Pigolotti S. Thermodynamics of Error Correction. *Phys Rev X.* 2015; 5(4):041039. doi: 10.1103/PhysRevX.5.041039.
- Scofano HM,** Vieyra A, de Meis L. Substrate regulation of the sarcoplasmic reticulum ATPase. Transient kinetic studies. *J Biol Chem.* 1979; 254(20):10227–10231. doi: 10.1016/S0021-9258(19)86697-8.
- Siess EA,** Brocks DG, Wieland OH. Subcellular distribution of key metabolites in isolated liver cells from fasted rats. *FEBS Lett.* 1976; 69(1):265–271. doi: 10.1016/0014-5793(76)80701-6.
- Soman S,** Keatinge M, Moein M, Da Costa M, Mortiboys H, Skupin A, Sugunan S, Bazala M, Kuznicki J, Bandmann O. Inhibition of the mitochondrial calcium uniporter rescues dopaminergic neurons in pink1^{-/-} zebrafish. *Eur J Neurosci.* 2017; 45(4):528–535. doi: 10.1111/ejn.13473.
- Stettner AI,** Segrè D. The cost of efficiency in energy metabolism. *Proc Natl Acad Sci USA.* 2013; 110(24):9629–9630. doi: 10.1073/pnas.1307485110.
- Thurley K,** Tovey SC, Moenke G, Prince VL, Meena A, Thomas AP, Skupin A, Taylor CW, Falcke M. Reliable Encoding of Stimulus Intensities Within Random Sequences of Intracellular Ca²⁺ Spikes. *Sci Signal.* 2014; 7(331):ra59–ra59. doi: 10.1126/scisignal.2005237.

- Visch HJ**, Koopman WJH, Zeegers D, van Emst-de Vries SE, van Kuppeveld FJM, van den Heuvel LWPJ, Smeitink JAM, Willems PHGM. Ca²⁺-mobilizing agonists increase mitochondrial ATP production to accelerate cytosolic Ca²⁺ removal: aberrations in human complex I deficiency. *American Journal of Physiology-Cell Physiology*. 2006; 291(2):C308–C316. doi: [10.1152/ajpcell.00561.2005](https://doi.org/10.1152/ajpcell.00561.2005).
- Wachtel A**, Rao R, Esposito M. Thermodynamically consistent coarse graining of biocatalysts beyond Michaelis–Menten. *New J Phys*. 2018; 20(4):042002. doi: [10.1088/1367-2630/aab5c9](https://doi.org/10.1088/1367-2630/aab5c9).
- Wachtel A**, Rao R, Esposito M. Free-energy transduction in chemical reaction networks: From enzymes to metabolism. *J Chem Phys*. 2022; 157(2):024109. doi: [10.1063/5.0091035](https://doi.org/10.1063/5.0091035).
- Wacquier B**, Combettes L, Van Nhieu GT, Dupont G. Interplay Between Intracellular Ca²⁺ Oscillations and Ca²⁺-stimulated Mitochondrial Metabolism. *Sci Rep*. 2016; 6:19316. doi: [10.1038/srep19316](https://doi.org/10.1038/srep19316).
- Wei AC**, Aon M, O'Rourke B, Winslow R, Cortassa S. Mitochondrial Energetics, pH Regulation, and Ion Dynamics: A Computational-Experimental Approach. *Biophys J*. 2011; 100(12):2894–2903. doi: [10.1016/j.bpj.2011.05.027](https://doi.org/10.1016/j.bpj.2011.05.027).
- Wikström M**, Springett R. Thermodynamic efficiency, reversibility, and degree of coupling in energy conservation by the mitochondrial respiratory chain. *Commun Biol*. 2020; 3(1):1–9. doi: [10.1038/s42003-020-01192-w](https://doi.org/10.1038/s42003-020-01192-w).
- Woods NM**, Cuthbertson KSR, Cobbold PH. Repetitive transient rises in cytoplasmic free calcium in hormone-stimulated hepatocytes. *Nature*. 1986; 319(6054):600. doi: [10.1038/319600a0](https://doi.org/10.1038/319600a0).
- Wu F**, Yang F, Vinnakota KC, Beard DA. Computer Modeling of Mitochondrial Tricarboxylic Acid Cycle, Oxidative Phosphorylation, Metabolite Transport, and Electrophysiology. *J Biol Chem*. 2007; 282(34):24525–24537. doi: [10.1074/jbc.M701024200](https://doi.org/10.1074/jbc.M701024200).
- Yang X**, Heinemann M, Howard J, Huber G, Iyer-Biswas S, Treut GL, Lynch M, Montooth KL, Needleman DJ, Pigolotti S, Rodenfels J, Ronceray P, Shankar S, Tavassoly I, Thutupalli S, Titov DV, Wang J, Foster PJ. Physical bioenergetics: Energy fluxes, budgets, and constraints in cells. *PNAS*. 2021; 118(26):e2026786118. doi: [10.1073/pnas.2026786118](https://doi.org/10.1073/pnas.2026786118).

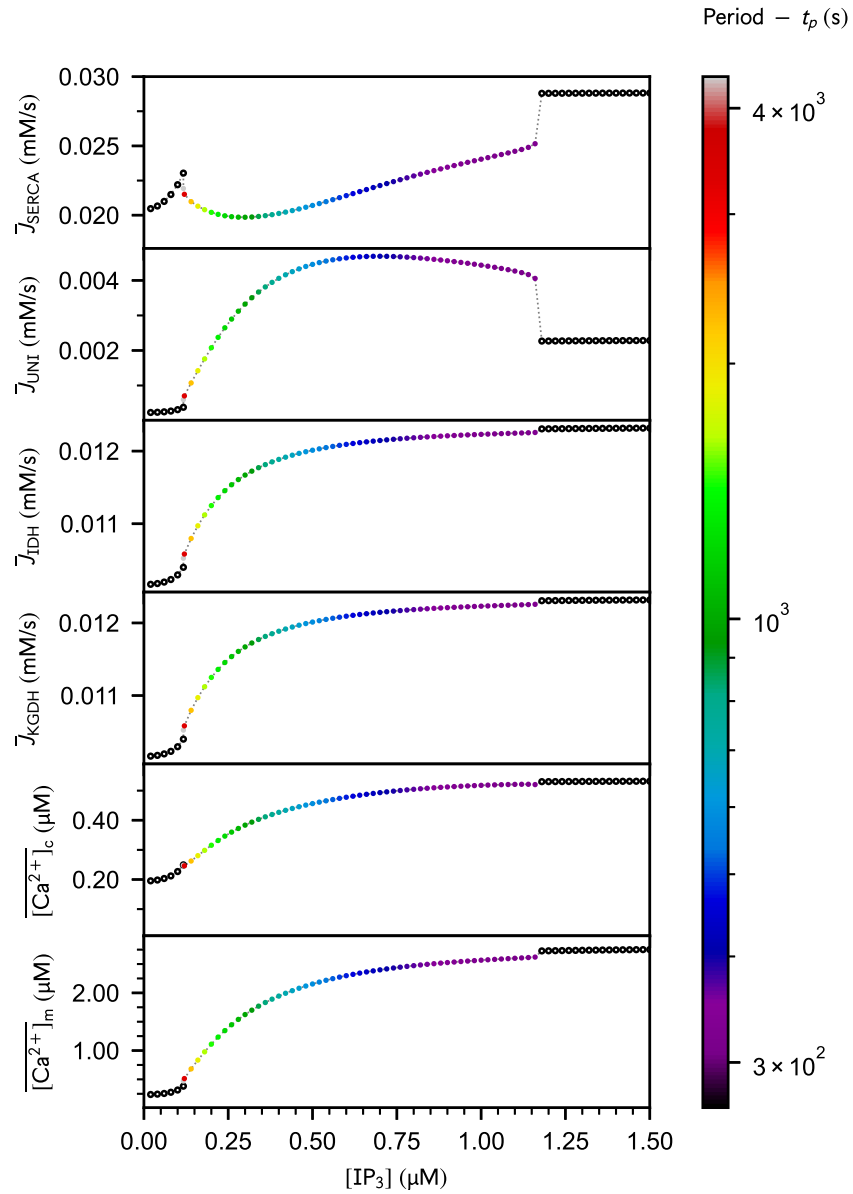


Figure 2—figure supplement 1. Average SERCA, UNI and Ca²⁺-dependent TCA fluxes and average cytosolic and mitochondrial Ca²⁺ concentrations vs. [IP₃] as complementary figures to the bifurcation diagrams shown in *Figure 2D* and *Figure 3C* bottom and portrait phases in *Figure 4C*. Note that \bar{J}_{IDH} and \bar{J}_{KGDH} are indistinguishable. Empty and filled dots correspond to steady-state or period-averaged quantities, respectively. Parameter values are the same as in *Figure 2D*.

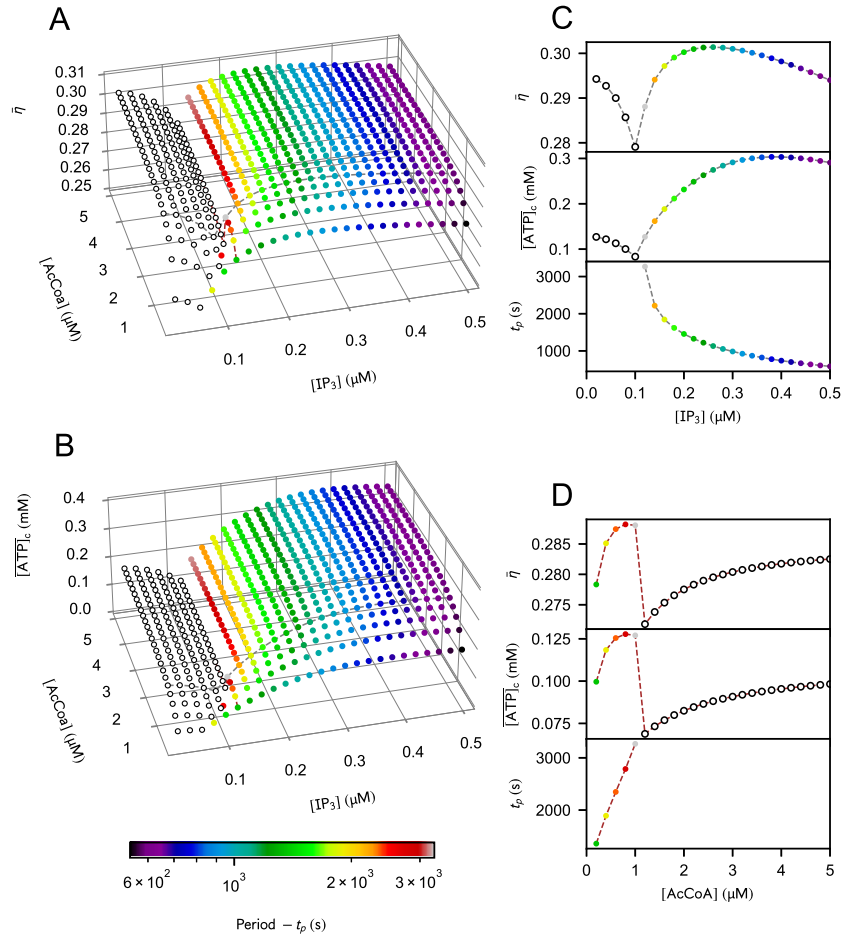


Figure 3—figure supplement 1. Efficiency of mitochondrial metabolism (η), average cytosolic ATP concentration ($\overline{[\text{ATP}]_c}$ (mM)) and period of Ca²⁺ oscillations (t_p) as functions of [AcCoA] and [IP₃]. (A-B) Summary 3D plots. IP₃ plays a dominant role in the transition between steady-state and oscillations, which usually takes place for concentrations of IP₃ between 0.1 and 0.2 μM . The onset of oscillations can be triggered for smaller [IP₃] in the presence of a very low level of AcCoA (e.g. [AcCoA] = 0.2 μM), which supports the role of Ca²⁺ oscillations as a rescuing mechanism aiming to improve the efficiency of energy production in stressing situations such as limited access to carbon substrate. For more clarity, representative behaviors of the efficiency (top panels), $\overline{[\text{ATP}]_c}$ (mM) (middle panels) and period (low panels) were plot for (grey lines - C) [AcCoA] = 1 μM and (brown lines - D) [IP₃] = 0.12 μM , as complementary figures to the bifurcation diagrams shown in Fig. 2E and 2F, respectively. Note that maxima in efficiency and in $\overline{[\text{ATP}]_c}$ (mM) can also be observed when [AcCoA] is varied. Increments in concentrations are of 0.2 μM (A-B) or 0.1 μM (D) for AcCoA and of 0.2 μM (A - C) for IP₃.

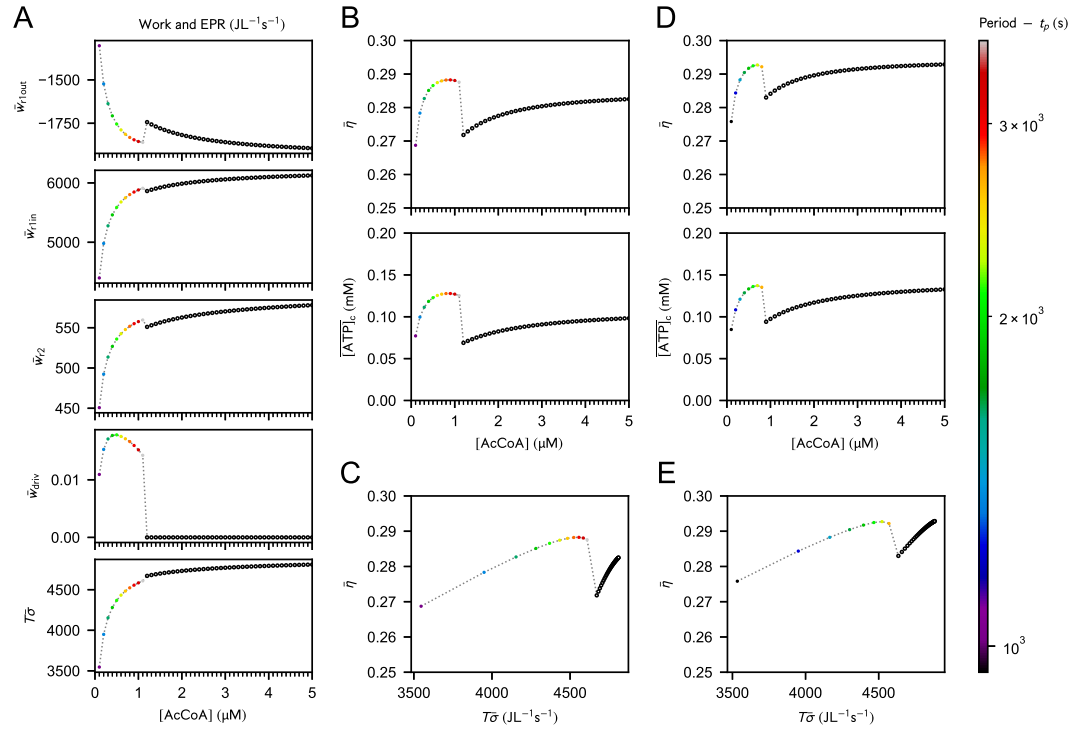


Figure 3—figure supplement 2. Stimulation of mitochondrial metabolism by AcCoA impacts Ca²⁺ dynamics *via* the Ca²⁺-metabolism crosstalk. (A) Nonconservative work contributions, driving work and dissipation for different [AcCoA]. The driving work represents less than 0.0004% of the EPR. At high stimulation, oscillations disappear in the favor of a nonequilibrium steady-state regime. (B) Efficiency and ATP_c concentration as a function of [IP₃]. (C) Efficiency as a function of the total dissipation for the same range of [AcCoA] as in (A) and (B). (D-E) Plots corresponding to (B-C) for $V_{max}^{SERCA} = 0.08 \mu\text{M s}^{-1}$. Empty and filled dots correspond to steady-state or period-averaged quantities, respectively. Unless specified otherwise, parameter values are the same as in Figure 2D.

This figure "frog.jpg" is available in "jpg" format from:

<http://arxiv.org/ps/2303.08822v3>